Multi-parametric imaging for tumor longitudinal follow-up

by

Maxime Doury

from the Laboratoire d'Imagerie Biomédicale

Submitted to the Université Pierre et Marie Curie (Paris VI)
in partial fulfillment of the requirements for the degree of

Doctor of Physics

September 2017

Author .....
Laboratoire d'Imagerie Biomédicale
September 1, 2017

Certified by .....
Frédérique Frouin
IMIV, Inserm, Paris Sud
Thesis Supervisor

Certified by .....
Alain de Cesare
LIB, CNRS, UPMC
Thesis Supervisor

Accepted by .....
William M. Deen
Chairman, Department Committee on Graduate Students

Multi-parametric imaging for tumor longitudinal follow-up

by

Maxime Doury

Submitted to the Université Pierre et Marie Curie (Paris VI)
on September 1, 2017, in partial fulfillment of the
requirements for the degree of
Doctor of Physics

Abstract

In this thesis, I discuss the application and development of methods for the automated discovery of motifs in sequential data. These data include DNA sequences, protein sequences, and real–valued sequential data such as protein structures and timeseries of arbitrary dimension. As more genomes are sequenced and annotated, the need for automated, computational methods for analyzing biological data is increasing rapidly. In broad terms, the goal of this thesis is to treat sequential data sets as unknown languages and to develop tools for interpreting an understanding these languages.

The first chapter of this thesis is an introduction to the fundamentals of motif discovery, which establishes a common mode of thought and vocabulary for the subsequent chapters. One of the central themes of this work is the use of grammatical models, which are more commonly associated with the field of computational linguistics. In the second chapter, I use grammatical models to design novel antimicrobial peptides (AmPs). AmPs are small proteins used by the innate immune system to combat bacterial infection in multicellular eukaryotes. There is mounting evidence that these peptides are less susceptible to bacterial resistance than traditional antibiotics and may form the basis for a novel class of therapeutics. In this thesis, I described the rational design of novel AmPs that show limited homology to naturally–occurring proteins but have strong bacteriostatic activity against several species of bacteria, including *Staphylococcus aureus* and *Bacillus anthracis*. These peptides were designed using a linguistic model of natural AmPs by treating the amino acid sequences of natural AmPs as a formal language and building a set of regular grammars to describe this language. This set of grammars was used to create novel, unnatural AmP sequences that conform to the formal syntax of natural antimicrobial peptides but populate a previously unexplored region of protein sequence space.

The third chapter describes a novel, GEneric MOtif DIscovery Algorithm (Gemoda) for sequential data. Gemoda can be applied to any dataset with a sequential character, including both categorical and real–valued data. As I show, Gemoda deterministically discovers motifs that are maximal in composition and length. As well, the algorithm allows any choice of similarity metric for finding motifs. These motifs are representation–agnostic: they can be represented using regular expressions, position weight matrices, or any other model for sequential data. I demonstrate a number of applications of the algorithm, including the

discovery of motifs in amino acids and DNA sequences, and the discovery of conserved protein sub–structures.

The final chapter is devoted to a series of smaller projects, employing tools and methods indirectly related to motif discovery in sequential data. I describe the construction of a software tool, Biogrep that is designed to match large pattern sets against large biosequence databases in a *parallel* fashion. This makes biogrep well–suited to annotating sets of sequences using biologically significant patterns. In addition, I show that the BLOSUM series of amino acid substitution matrices, which are commonly used in motif discovery and sequence alignment problems, have changed drastically over time. The fidelity of amino acid sequence alignment and motif discovery tools depends strongly on the target frequencies implied by these underlying matrices. Thus, these results suggest that further optimization of these matrices is possible.

The final chapter also contains two projects wherein I apply statistical motif discovery tools instead of grammatical tools. In the first of these two, I develop three different physiochemical representations for a set of roughly 700 HIV–I protease substrates and use these representations for sequence classification and annotation. In the second of these two projects, I develop a simple statistical method for parsing out the phenotypic contribution of a single mutation from libraries of functional diversity that contain a multitude of mutations and varied phenotypes. I show that this new method successfully elucidates the effects of single nucleotide polymorphisms on the strength of a promoter placed upstream of a reporter gene.

The central theme, present throughout this work, is the development and application of novel approaches to finding motifs in sequential data. The work on the design of AmPs is very applied and relies heavily on existing literature. In contrast, the work on Gemoda is the greatest contribution of this thesis and contains many new ideas.

Thesis Supervisor: Frédérique Frouin
Title: IMIV, Inserm, Paris Sud

Thesis Supervisor: Alain de Cesare
Title: LIB, CNRS, UPMC

Acknowledgments

I am indebted to many people who both directly and indirectly contributed to this thesis. First, I would like to thank those collaborators who directly contributed. Most of all, I'm grateful for the help and friendship of Mark Styczynski. Mark was my collaborator on all matters computational for the past four years — his influence is evident throughout this document. I'm also grateful for my collaboration with Christopher Loose, who performed many of the experiments on antimicrobial peptides described in Chapter **??**. Finally, I would like to thank Isidore Rigoutsos, who straddled the line between collaborator and advisor. Isidore taught me an attention to detail and a penchant for the UNIX command line and vi editor.

Most importantly, I am indebted to Greg Stephanopoulos, my advisor, whose guidance and support was unwavering these past six years. Greg is the perpetual optimist — always positive in the face of my many failures along the way. He also gave me the freedom to pursue projects of my own choosing, which contributed greatly to my academic independence, if not the selection of wise projects.

I am much obliged to my thesis committee members: my advisor Greg, Isidore, Bill Green, and Bob Berwick. My committee was always flexible in scheduling and judicious in their application of both carrots and sticks.

There are numerous people who contributed indirectly to this thesis. First among these is my intelligent, lovely, and vivacious wife Kathryn Miller–Jensen. Next, my parents Carl and Julie, my sister Heather, and my in-laws, Ron, Joyce, Suzanne, Jeff, and Mindi. Finally, there are innumerable friends who contributed and to whom I am greatly appreciative including Michael Raab, Joel Moxley, Bill Schmitt, Vipin Guptda, and Jatin Misra.

Contents

List of Figures

List of Tables

Chapter 1

Introduction to cancer monitoring and perfusion imaging

1.1 Context

1.1.1 Cancer and tumor microenvironment

Cancer: what's in a name?

A brief history of cancer.

1.1.2 Treatment of cancer

1.1.3 Cancer monitoring

1.2 Perfusion imaging

1.2.1 Generalities on perfusion imaging

1.2.2 Nuclear Medicine

1.2.3 Magnetic resonance (MR)

1.2.4 X-ray computed tomography (CT)

1.2.5 Contrast-enhanced ultrasound (CEUS)

Chapter 2

Quantification of perfusion exams: A review

Generally speaking, quantification of perfusion consists in deriving parameters from blood flow measurements, regardless of the method used for the measure. This topic has been on the table, and continuously evolving, long before perfusion imaging existed. Indeed, G.N. Stewart introduced indicator dilution theory, starting with the founding paper published in the Journal of Physiology in 1897 [51]. W.F. Hamilton went further, corrected the approximations made by Stewart. Even before Stewart and Hamilton, hemodynamics of the heart had been studied through indirect measurements and reported in German language by Volkmann [67] and Vierordt [66] in the 1850s, and later through direct measurements by Stolnikow [52] and Tigerstedt [62].

This chapter fundamentally aims to review the various methods used to quantify perfusion exams acquired using one of the imaging modality described in Chapter 1.2. Realistically, this review of perfusion quantification techniques cannot be close to comprehensive, instead it tackles the subject from the three angles mentioned thereafter, and emphasis the major landmarks of the perfusion quantification landscape.

Section 2.1 presents semi-quantitative methods, extracting parameters directly either from raw or noise-filtered enhancement curves. Then Section 2.2 presents deconvolution-based quantification methods, estimating the vascular transfer function in the tissue of interest by means of blind or regularized deconvolution. Finally, compartmental models ac-

counting for the various interactions of the contrast agent with the tissue are presented in Section 2.3.

2.1 Semi-quantitative methods

2.1.1 Generalities

Semi-quantitative methods are probably among the most intuitive as they extract perfusion-related parameters directly from raw, interpolated, or noise-filtered enhancement curves. They are however not directly related to any physiological function and are prone to changes in experimental or physiological conditions. They are therefore often used as relative indicators of perfusion and contrast agent transit time [35], allowing intra-exam comparisons.

Examples of semi-quantitative parameters include the peak enhancement [14, 38, 39, 42], the time to peak enhancement [12, 14, 39], maximum upslope gradient, also known as wash-in rate [14, 38], the area under the enhancement curve [12], but also perfusion parameters based on indicator dilution theory based on the previously cited parameters [6, 21, 25, 33, 35, 36, 40, 41]. Figure **??** shows graphical representations of the above mentioned semi-quantitative parameters.

2.1.2 Nuclear medicine

Semi-quantitative parameters have been used to differentiate stenosed from healthy kidney in scintigraphy exams, i.e. a nuclear medicine technique using a gamma camera, following bolus injection of $[^{99m}Tc]$DTPA.

For instance, Hilson et al. and later Peters et al. both proposed an enhancement-based perfusion index, which is commonly defined as the ratio of the tissue blood flow to the cardiac output. On the one hand, Hilson et al. defined the perfusion index as the ratio of the area under the arterial curve to the area under the renal curve, both curves are integrated up to the arterial peak [21]. On the other hand, Peters et al. defined the perfusion index as the ratio of the maximum upslope of the renal curve normalized for the injected quantity to the maximum upslope of the integrated arterial curve normalized for the area under the arterial

enhancement curve, and multiplied by a constant converting the gamma camera into a unit of activity [40, 41].

Nally et al. reported significant differences in the wash-in rate, curve width at 75% of the peak enhancement, and maximum enhancement in normal and stenosed kidney in a canine model [38].

2.1.3 Radiography

Derived from the work of Peters et al., semi-quantitative parameters were also proposed by Miles et al. in 1991 to quantify renal cortical and medullary perfusion in X-ray computed tomography with bolus injection of Iodine [33, 35]. The proposed perfusion index was defined as the ratio of the maximum slope in the tissue curve and the peak enhancement of the arterial curve. The method was successively used to quantify perfusion in the pancreas [37], solitary pulmonary nodules [76], lymphoma masses [13], lung adenocarcinoma [54], and more generally to study tumor angiogenesis [34, 54].

Miles et al. also adapted the method to account for both arterial and venous perfusion of the liver, using the splenic enhancement as venous input because the portal vein was not present in the image [36]. Arterial perfusion was calculated using the maximum slope before peak splenic enhancement, while venous perfusion was calculated using the maximum slope after peak splenic enhancement.

In 1995 Blomley et al. proposed the liver subtraction method to quantify liver perfusion [6]. Instead of estimating the upslope in the late liver enhancement curve, they first subtracted the splenic enhancement curve multiplied by the ratio of arterial to splenic arterial perfusion, i.e. the ratio of the maximum slope in the early liver enhancement curve to the maximum slope in the spleen. The maximum slope of the corrected enhancement curve is then used to calculate portal perfusion. In this study, the time and value of peak enhancement were obtained using a gamma-variate fit, allowing a finer estimation of these parameters. Whenever possible the authors used the enhancement curve in the portal vein instead of the splenic vein. Authors demonstrated the use of portal perfusion in one patient with metastatic livers, as well as in four patients with cirrhotic livers. Facing the small number of cases in the previous study, a collaborating group extended the application of the

method in cirrhotic livers with more cases [63]. They estimated arterial and portal perfusion in a group of twenty patients with viral-induced cirrhosis and in fourteen controls. While arterial perfusion did not differ between groups, they found a significant reduction in portal perfusion among patients compared to controls, and a strong correlation between portal perfusion and the prothrombin ratio which is an indicator of hepatic parenchymal damage.

Inspired by the work of Miles et al., the method was adapted by Koenig et al. in 1998 to quantify perfusion in the brain in order to detect and assess cerebral ischemia in acute stroke [25]. While arterial enhancement could be estimated from small vessels present in the image, it was not used due to peak attenuation by partial volume effects. Instead, the peak venous enhancement in the superior sagittal sinus was used. The authors reported relatively small approximation error, with slightly flattened enhancement curves, explained by the short transit time of the contrast agent in brain tissues. The cerebral blood flow, commonly noted CBF, is the equivalent of the perfusion index in brain tissues. The authors defined it as the ratio of the maximum slope of the tissue enhancement curve to the peak enhancement in the superior sagittal sinus. The fractional cerebral blood volume, commonly noted CBV, was defined as the ratio of the peak tissue enhancement to the peak enhancement in the superior sagittal sinus. In a following study [24], the authors assess the linearity, the spatial resolution, and the sensitivity to noise of CBF through simulations and phantom study, and investigated the relative CBF estimated using large hemispherically mirrored regions of interest using follow-up CT and MR data. They reported a systematic underestimation of CBF correlated with the cardiac output of the patient, a good linearity of relative CBF, and recommend using the relative parameter as a predictor of the reversibility of an ischemic stroke.

2.1.4 Magnetic resonance imaging

Following the methodological developments of Gadolinium-DTPA complex (Gd-DTPA) by Brasch et al. [8], Weinmann et al. [70], and Wesbey et al. [71] in 1984 supported by qualitative visual analysis, various applications of the technique emerged in the field of oncology.

Quantification attempts started with the work of Felix et al. [17] in 1985 using Gd-DTPA enhanced images acquired 5 minutes after injection of the contrast agent. Results were compared with pre-contrast MR images obtained using various acquisition sequences and X-ray

computed tomography imaging with injection of a iodinated contrast agent. They obtained accurate contours of brain tumor and necrosis with no significant enhancement in the region exhibiting peritumoral edema. They also attempted to differentiate the various types of tumor included in their study based on the contrast index before and after injection of Gd-DTPA. The index is defined as the ratio of signal intensity in the tumor tissue to the signal intensity in normal brain tissue. It is the first semi-quantitative parameter used for Gd-DTPA enhanced MRI.

Revel et al. [47] assessed the difference in signal intensity between the pre-contrast and 25-minute post-contrast images acquired in the largest section of subcutaneous human breast tumors implanted in mice. Signal intensity in the tissue were normalized by the signal intensity in a corn-oil phantom visible in every image. Limited by the temporal resolution of their acquisition, authors do not comment on the temporal evolution of signal intensity, despite intermediate acquisitions performed respectively 5 and 15 minutes after Gd-DTPA injection.

Pettersson et al. [42] performed repeated acquisitions of multiple MR sequences in rabbits subcutaneously implanted with a Vx2 tumor model, and additional induced hemorrhage in surrounding muscle tissue. Temporal evolution of enhancement is assessed more finely than in previous studies, acquiring an image every 2.5 minutes for the first 10 minutes after injection of Gd-DTPA and then every 5 minutes for the following 20 minutes. This allowed the authors to observe that no substantial enhancement occurred in abnormal tissues after 10 minutes, however they only reported on variations of peak signal intensity.

In 1989, Erlemann et al. [14] investigated dynamic contrast-enhanced MRI using a T1-weighted spin-echo sequence every 20 seconds following bolus injection of Gd-DTPA as a tool to differentiate tumors from healthy tissue in musculoskeletal lesions. Their primary result was an increase in contrast-to-noise ratio between tumor and muscle compared to T2-weighted images, and a decrease in contrast-to-noise ratio between tumor and bone marrow or fatty tissue compared to non-enhanced T1-weighted images. Additionally, they estimated the baseline signal intensity, the maximum signal intensity, and the time-lapse between the start of the injection and the point of maximum signal intensity. Using these estimates, the defined the signal intensity ratio as the percentage of increase over the baseline signal in-

tensity, as well as the relative enhancement slope. They observed an increase of the signal intensity ratios and relative enhancement slope in malignant tumors compared to benign tumors, the latter showing smaller overlap between malignant and benign groups. Enhancement slope enabled malignancy prediction with an accuracy of 79.7% using a cutoff value of 30%/min. They also reported lower peak intensity ratios and wash-in rates in areas with necrosis or peritumoral edema.

Verstraete et al. [65] also reported on the ability to differentiate benign from malignant musculoskeletal lesions, using imaging and quantification techniques similar to those used by Erlemann et al. [14]. Despite the higher temporal resolution of 2.41 seconds possible in their study, their findings are likewise nuanced because of the overlap of parameters between highly vascularized benign lesions and the malignant ones.

Baur et al. [4] reported higher signal intensity ratios after injection of Gd-DTPA in patients with intermediate-grade and high-grade diffuse malignant bone marrow infiltration in the spine compared to healthy patients. Nonetheless, they were unable to detect low-grade lesions using this technique, and reported large variabilities in all patient groups.

2.1.5 Ultrasound imaging

The current section addresses the semi-quantitative methods used to quantify perfusion using ultrasound. Refer to Section 1.2.5 for more information on contrast-enhanced ultrasound as a perfusion imaging modality, including the nature of the contrast-agent, the image formation processes, as well as the various injection techniques. Methods assessing perfusion using bolus injection are first presented, followed by methods specific to continuous infusion injection.

As a foreword to this section, indicator dilution theory as first formalized by Stewart [51] and later by Hamilton et al. [19] is valid under the condition that the mass of contrast-agent is conserved through the time of the acquisition. Since 1979, it a known that a portion of the intravenously injected microbubbles are filtrated through the lungs [10] , i.e. before their first pass in the tissue of interest. Moreover, a portion of the following passes is filtered by the Kupffer cells in the liver [23, 75]. Additionally, Lampaskis and Averkiou [29] confirmed that imaging using a high mechanical index disrupts a non-negligible number of

microbubbles, and demonstrated that most of the microbubbles disrupted during imaging at a low mechanical-index are actually naturally disrupted. The mass conservation condition is therefore usually not respected in contrast-enhanced ultrasound, even in first-pass studies. Semi-quantitative methods based on indicator dilution theory were nonetheless extensively used to quantify perfusion in contrast-enhanced ultrasound exams.

Bolus injection

Model-free quantification methods

From an historical standpoint, Bommer et al. [7] were the first to report indicator-dilution curves using contrast-enhanced ultrasound data in an abstract published in The American Journal of Cardiology in 1978. Authors used a photometer to quantify the evolution of signal intensity, as visualized on the screen of the monitor. The enhancement resulted from the venous injection of a bolus of microbubbles, obtained by microcavitations through rapid injection of dextrose in water. The indicator-dilution curves were quantified in terms of time from peak enhancement to 50% decay, and to 90% decay. The latter was found correlated to the cardiac-output, and enabled the differenciation of patients with low and normal cardiac index. In the same issue of The American Journal of Cardiology, the same group applied the same technique to produce indicator-dilution curves in another cardiac study [11]. They used the ultrasound images themselves to identify patients with intracardiac shunts, but also the mean clearance time of the indicator-dilution curves to identify patients with tricuspid regurgitation, and severe congestive failure.

At the same period, Hagler et al. [18] presented early data of videodensitometry data for the quantification of left-to-right shunts using echographic acquisitions with direct injection of a bolus of ultrasound contrast-agent (i.e. indocyanine green dye) in the left ventricule. They estimated the ratio of left-to-right shunt, which they defined as the ratio of the area under the curve in the right ventricule to the area under the curve in the left ventricule, and showed an strong correlation of echographic measurements with both indicator-dilution and dye measurements. Meltzer et al. [32] extended this work and investigated the relevance of a mono-exponential model to fit the wash-out curve, as suggested by indicator-dilution theory. This was assessed by fitting a linear model to the log-transformed time-density wash-

out curve, exhibiting excellent correlation with experimental data. They therefore concluded on the relevance of the slope in the linear model, and established its relation to the contrast agent disapearance rate.

Following the early work of Armstrong et al. [1] and Tei et al. [55], Ten Cate et al. [56] investigated the use of contrast-enhanced echography for the assessment of myocardial perfusion following intracoronary injection of a bolus injection of microbubbles in a canine study with varying coronary artery flow (using a hydraulic occluder) to simulate ischemia, and with injection of Dipyridamole to dilate the coronary bed and therefore simulate hyperemia. The microbubbles in this study were investigated in a previous study of the same group, ensuring they were small enough to circulate through capillaries without getting trapped [16]. Semi-quantitative functional parameters were extracted from log-compressed time-intensity curves, i.e. the half wash-in time, half wash-out time (ignoring recirculation fitting a mono-exponential model), peak intensity time and value, and total curve duration. They found significant changes in total curve duration, and in half wash-in and wash-out times, for both ischemia and hyperemia in comparison with control measurements. Inter-observer and intraobserver variability, as well as injection reproducibility was assessed for the half wash-out time, with respective correlation coefficients of 0.98, 0.86, and 0.78. In addition, the relative systolic wall thickening was also estimated, and while it correlated well with the coronary artery flow measured by an electromagnetic flowmeter placed directly on the artery, no correlation was foud with the half wash-out time.

A few years later, Vandenberg et al. [64] performed a similar canine study with induced ischemia and hyperemia, intending to predict myocardial blood flow from semi-quantitative parameters derived from contrast-enhanced ultrasound time-intensity curves. In addition to peak intensity time and value, they investigated the use of the wash-in rate. Peak intensity value and wash-in rate were found correlated to myocardial blood flow, however correlations were moderate (r = 0.67 and 0.51 respectively). However, the relative changes of the wash-in rate exhibited a stronger correlation (r = 0.77) with the relative changes of the myocardial blood flow, i.e. with induced ischemia and hyperemia.

In a clinical study, Ten Cate et al. [57] estimated the total curve duration, the area under the curve, and the half wash-out time from time-intensity curves obtained in the ventricu-

lar septum from end-diastolic images. They performed multiple regression analysis between the parameters extracted from contrast-enhanced ultrasound data to angiographic parameters, i.e. the percentage of coronary area stenosis, and the minimal lumen area, derived from data acquired using the protocol described in [73]. Authors reported relations of various natures between the above-mentioned parameters, i.e. linear, inverse, exponential, and logarithmic. In particular, the strongest correlation was found between the area under the curve and the percentage of coronary area stenosis (exponential relation). Additionally, while all correlation were found significant, this couple of parameters was the only one with a strong correlation ($r \geq 0.8$). Noting the discrepencies between the pre-clinical and the clinical results, the authors suggest they found their sources in modifications of the experimental setup, i.e. the injection method or the nature of the ultrasound contrast agent.

In 1990, Bleeker et al. [5] evaluated the stability, size, and ultrasonic properties of multiple ultrasond contrast agents, and investigated the feasibility of blood flow estimation through in-vitro experiments. Their findings were in favor of the Albunex contrast agent, which were the only microbubbles exhibiting sufficiently longlasting stability (i.e. in size and number) when exposed to ultrasound waves. In addition, a linear relation between the concentration of microbubbles and both backscatter coefficient (i.e. reflected power) and attenuation coefficient (i.e. transmitted power) was reported for low concentrations. They also found strong linear relations between the ultrasonic properties of the contrast agent and the flow estimated using an indicator-dilution theory. They emphasis the questionability of using grey-levels from ultrasond images to characterize blood flow, and instead recommend using attenuation based on transmission techniques, or backscattering after proper correction of signal attenuation. While in-vitro experiments show strong relations between the ultrasonic properties of Albunex contrast agent and the flow estimated using indicator-dilution theory, one must consider the mass conservation principle which is rarely respected in-vivo.

A somehow similar in-vitro study was conducted a few years later by Heidenreich et al. [20], however the proposed quantification model makes use of an input function as a reference instead of the injected quantity used by Bleeker et al. [5], and extends the indicator-dilution model to estimate the tissue blood volume and mean transit time, in addition to the tissue blood flow. The model is based on the estimation of the area under the curve and

mean transit time for both input and studied tissues. The ratio of the area under the curve in the studied tissue to the input yields the tissue blood volume, the system mean transit time is approximated as twice the difference in mean transit times, and the tissue blood flow was classically defined as the ratio of tissue blood volume to system mean transit time. In-vitro calibration data revealed the log-compressed nature of the data in the experimental system, allowing linearization of the video intensity for low to moderate concentrations, and therefore conversion to volumetric concentration of microbubbles. Excellent agreement was found between measured and estimated flow rates, using 39 measurements at low concentration. Authors report on the difficulty to find a pure blood pool in the ultrasound imaging plane, but also to image both tissue and input with sufficient sensitivity and without saturation artifacts respectively because of the limited dynamic range of commercial ultrasound scanners. Additionally they comment on the simplicity of the model which allows to alleviate the signal attenuation artifacts which are often non-negligible in-vivo, and on the impossibility to ensure conservation of the contrast agent quantity and properties throughout the acquisition.

Aronson et al. [2], from the same research group, later assessed the model described above in-vivo, in an attempt to quantify kidney perfusion in a canine study. A total of 58 bolus injections of microbubbles with varying concentrations (23 for aortic measurements, and 35 for cortical measurements), and 93 bolus injections with modulated blood flow (57 reduction, 10 increase, and 26 controls), were performed in 9 dogs. Blood flow was controled by means of a renal artery occluder for flow reduction, and dopamine or fenoldopam infusion for flow increase. A major limitation of this study lies in the fact that renal and aortic data did not originate from the same injection, as a different dose of contrast-agents was used to extract the time-intensity curves in the two regions of interest. Additionally, the injected doses were ajusted empirically in order to obtain complete opacification of the region of interest, without reaching the signal saturation threshold. Direct measurements of blood flow were performed using an electromagnetic flowmeter, for comparison with the value estimated using contrast-enhanced ultrasound. The major findings of this study are the evidence of a strong correlation between the injected concentration and the pixel intensity, for both cortical and aortic measurements, and strong correlation of the estimated

blood flow with in-situ flow measurements with a tendency to overestimate blood flow. Authors discuss the various pitfalls of contrast-enhanced ultrasound that could influence the accuracy of the method, including possible changes in blood volume in the modulated flow experiments, signal attenuation, and electronic thresholding. They finally conclude on the inability to perform absolute quantification of blood flow with the existing apparatus, stating that the major requirements lie in increased linearity and dynamic range.

Schwarz et al. [49] investigated the use of the wash-out rate from log-transformed time-intensity curves following bolus injection, as well as the ratio of the wash-out rates from two bolus injections with varying flow rates. Time-intensity curves were obtained using various backscatter intensity techniques, i.e. radio frequency, video intensity, pulsed wave Doppler, and intravascular Doppler. Authors obtained strong correlations of the wash-out rate with the in-vitro flow rate, however they reported different slopes in two chambers with varying mixing volume. The relative wash-out rate not only exhibited excellent correlations with the relative flow rate, it also yielded a good agreement of the slopes obtained in the two mixing chambers. These results suggest the independence of the relative wash-out rate to the mixing volume, and the ability of this parameter to accurately characterize changes in blood flow.

Wiencek et al. [72] investigated the various steps necessary to achieve accurate quantification of contrast echocardiography using indicator-dilution theory. The proposed approach relies on the knowledge of an arterial input function, i.e. the time-intensity curve in a pure blood pool like the aortic root or in the left ventricle, in order to relax the need for standardized injection and physiological conditions. Authors ackowledge the difficulty of estimating the input function using a single injection, and suggest performing two separate injections to avoid saturation and non-linearities caused by high contrast-agent concentrations. They emphasis the necessity for a consistent and confined range of microbubble size, as the intensity of the signal backscattered by a single bubble is non-linearly proportional to the diameter of the bubble. The importance of conservation of contrast-agent quantity and properties throughout the acquisition of the ultrasound images was outlined, and the impact of hydrostatic pressure and gas saturation level of the solution as reported in the litterature was investigated. The choice of the representation of the time-intensity curves, i.e. video intensity, log-transformed intensity, or concentration from calibration data, and its

impact on the estimated parameters were discussed. A possible explaination for undetected changes when using peak height as an indicator of blood flow was proposed, authors related it to signal saturation and illustrate this phenomenum in simple cases where the changes in blood flow are caused by a change in blood volume only or in transit time only. Additionally, electronic issues resulting from signal acquisition, signal processing, and electronic thresholding were discussed. Physiological factors like tissue-dependant hematocrit were also investigated. Finally, methods which showed promising results in preliminary studies at the time of the review (i.e. 1993) were reported, including various alternative imaging schemes (e.g. acoustic velocity, radiofrequency data, second harmonic imaging).

Model-based quantification methods

In 1989, Kaul et al. [22] proposed a first-order gamma-variate model to quantify blood flow using consecutive contrast-enhanced echocardiography acquisitions in an open-chest canine study with varying blood flow. They compared their results in the myocardium and in the coronary bed with the transmural myocardial blood flow measured using radiolabelled microspheres, and to direct coronary flow measurements obtained by an electromagnetic flowmeter. They studied the influence of the injection site by performing their experiments in two groups of eight dogs. In the first group, dogs were injected a bolus of microbubbles in the circumflex artery, while in the second group they were injected in the left main coronary. Authors reported a good correlation of both myocardial and coronary blood flow measurements with the parameter of the gamma-variate which influences the curve width, α, for both groups (mean r = 0.81 and 0.96 respectively), but a poor correlation of the peak intensity (mean r = 0.63 and 0.39 respectively). Pooling estimates from the eight dogs did not affect the correlation with α for the first group (r = 0.80), however for the second group, pooling data considerably dropped the correlation (r = 0.23). Scattered plots reveal the varying slopes obtained in the different dogs, emphasizing the impact of the injection site. Indeed, when injecting in the left main coronary the contrast agent is dispersed throught the coronary tree, making quantification of myocardial blood flow intrinsically relative. Authors suggested that absolute quantification of myocardial blood flow may be possible, injecting closer to the branches of the coronary tree, but were well aware that the proposed semi-

quantitative parameters are not absolute themselves.

Tiemann et al. [59] investigated the ability of harmonic power Doppler imaging to yield quantitative perfusion parameters, as this modality inherently destroys microbubble to produce contrast-specific images [60], through in vitro experiments, and ex vivo experiments in a porcine heart. They compared the time-intensity curves obtained from harmonic power Doppler, and the time-concentration curves of ICG measured with an extravascular densitometer, to direct flow measurements from a calibrated ultrasonic flowmeter. Authors fitted a log-normal model to the experimental curves, since this model has been commonly used to fit indicator-dilution curves [53, 74], and was later applied in cardiology studies [3, 30]. The area under the curve and the mean transit time of the fitted model were estimated for both modalities. While the area under the curve expectedly correlated with the injected quantity of ultrasound contrast agent, the inverse of the mean transit time obtained using microbubbles and ICG measurements exhibited very strong correlation to the direct flow measurements in both in vitro and ex vivo setups. However, the mean transit time obtained with harmonic power Doppler time concentration curves was slightly lower than with ICG densitometry, especially for high flow rates. While most studies used electromagnetic flowmeters as ground truth, this one used an ultrasonic transit-time flowmeter. The presence of ultrasonic microbubbles could therefore influence the ground truth flow measurement, and possibly affect the correlation between ultrasonic measurements, however measurements were in accordance with densitometric ICG measurements which alleviates the suspicion.

In 2000, Postert et al. [43] proposed an empirical model for the quantification of cerebral perfusion time-intensity curves following intravenous injection of a bolus of microbbubles, imaged through the acoustic temporal bone window using phase-inversion harmonic ultrasound imaging, contrast burst imaging, and time variance imaging for comparison. The model accounts for the baseline-intensity and for the maximum change in intensity, i.e. the peak-intensity minus the baseline-intensity. Moreover, the wash-in of the bolus is modeled by a delayed sigmoid with adjustable slope, despite authors describe it as step function, and the destruction of microbubbles is modeled by an exponential decay. However, none of the model parameters is directly related to the physiology or to physical measurements. Authors used the peak-intensity, as well as the time to peak-intensity extracted parameters from the

modeled time-intensity curves as semi-quantitative parameters to compare the values obtained using the three modalities of contrast-enhanced ultrasond cited above, and in four regions of interest of nine healthy patients. The study concludes by stating the higher sensitivity of contrast burst imaging and time variance imaging compared to phase-inversion harmonic imaging.

However, three years later, a study by Eyding et al. [15] to which Postert collaborated, investigated the 90% peak width as an additional parameters to characterize time-intensity curves from phase-inversion harmonic imaging fitted with this model. Semi-quantitative parameters were evaluated in five regions of interest of the established unilateral view, i.e. with an imaging depth of 100 mm, and nine regions of interest using a novel the bilateral view including both hemishperes, i.e. with an imaging depth of 150 mm, of fourteen healthy patients. Consecutive transtemporal acquisitions following intravenous injection of two different ultrasound contrast agents were performed in each view of each patient, with twenty minute intervals, with for comparison purposes. The authors reported the sensitivity of peak-intensity to depth, and the ability to differentiate arteries using either time parameter.

In a following study [28], the same group performed another transtemporal contrast-enhanced ultrasound study using the bilateral approach with a single bolus injection in twenty healthy patients. A total of fourteen regions of interest was delineated in both hemishperes, yielding as many time-intensity curves, from which were estimated the same three semi-quantitative parameters after fitting the empirical model described above. Peak intensity was once again excluded from further analysis because of the strong variations among patients. Because of the small amount of corresponding regions in the study, only descriptive data is presented in the form of aligned boxplots, as if all patients exhibited the same median value. The authors recommended the use of the time parameters, in particular the time to peak intensity, as estimated with the bilateral protocol. They believe it could be a relevant indicator to help characterize lesions in patients with acute strokes, provided that one of the hemispheres is unaffected and can be used as a reference.

Infusion injection

In 1998, Wei et al. [68] proposed an explicit model to quantify myocardial perfusion. For this method, microbubbles were injected as a continuous infusion. When the micro-bubble concentration reached a steady state, high mechanical index ultrasound pulses were used to disrupt microbubbles in the myocardium with increasing pulsing interval. This technique is known as intermittent imaging. The video intensity, which was assumed proportional to the concentration in microbubbles, was plotted as a function of the pulsing interval. Then an exponential function with plateau value A and rate constant β was fitted. Assuming a constant beam elevation, Wei et al. [68] demonstrated that blood flow F was proportional to the slope at the origin, i.e. $A\beta$. The authors validated their approach in vitro, but also ex vivo and in vivo in a canine study. The method was later validated for perfusion quantification of the kidney, estimating both cortical and medullary blood flow in another canine study [69].

The development of power pulse inversion imaging by Simpson and Burns [50] in 1997, allowing real-time imaging of low microbubble concentration at low mechanical index [61]. Tiemann and Becher [58] in 2000 and Masugata et al. [31] in 2001 demonstrated the use of power pulse inversion to image the replenishment of tissue following a single series of microbubble-disrupting pulses in real-time. Both study also reveal that the model proposed by Wei et al. could be used to accurately fit real-time replenishment curves.

In 2001, Schlosser et al. [48] applied the same model to quantify renal perfusion, and compared the estimated parameters according to the acquisition sequence, i.e. power pulse inversion [50] vs. pulse inversion [9]. The authors disclosed highly different perfusion parameter values according to the acquisition scheme, which yielded significantly different values of both parameters. However, they were able to distinguish large arteries in the renal hilum from smaller arteries in the renal cortex, using either of the schemes, and either of the parameters.

In 2003, Krix et al. [26] presented a hyperbolic model to quantify perfusion using either intermittent or real-time imaging, relying on physiological considerations, and accounting for the distribution of blood velocities in the tissue. The model assumes a spherical distribution of blood vessel directions with varying blood velocity. This assumption yields an initial

linear increase of the concentration until the vessels perpendicular to the imaging plane with the highest velocity are fully refilled. After the initial linear increase in signal intensity, the fully filled vessels do not contribute to signal increase anymore. This yields a non-linear increase until only the vessels with the lowest velocity remain to be fully filled. Finally, all the vessels present in the imaging plane are fully filled and a plateau intensity is reached. Authors describe an iterative method to estimate the instant of maximum and mean velocity. They state the slope of the replenishment curve observed at these times can be used to evaluate the maximum blood velocity in the region of interest, assuming the width of the ultrasound beam is known. The influence on the width of the blood velocity distribution is visually described. The method was evaluated in a murine study with continuous infusion and intermittent imaging, followed by a bolus injection and intermittent imaging as well [27].

Potdevin et al. [44] investigated the misfit of the exponential model to refill curves and proposed the use of the error function instead. They introduced a time-delay parameter in their model in order to better reflect experimental data. They also investigated the impact of observing multiple blood velocities in the region of interest, as well as the effect of the point spread function of the imaging system through a simulation study and concluded that replenishment curves contain more information that just mean transit time. For instance they were able to reveal the presence of abnormal vascular structures, such as shunting, i.e. direct flow from the arterial system to the venous system without passing through the capillary bed. In a latter study, they proposed an adaptation of the model to quantify local replenishment curves in tissues with complex vascular structures. Replenishment curves are first normalized according to the estimated depth-dependent pixel intensity in a pixel containing only blood. The model accounts for the specific angles, lengths, and velocities of the various vascular structures in the studied tissue [45]. They also used their model as a tissue classifier tool, determining tissue type as the predefined vascular model that best fitted the enhancement curve in the least squares sense. However, applying the simpler exponential model with the average tissue mean transit time on normalized data yielded accurate tissue classification maps, suggesting that the major factor differentiating the replenishment curves of the various tissue types is actually mean transit time. The additional information

could be used to characterize vascular properties more finely. In spite, while their is no physical evidence why the exponential model should fit replenishment curves, it remains a good approximation and allow accurate differentiation among tissue types. This is especially true when applied to noisy replenishment curves.

?] introduced a new formalism for the quantification of real-time destruction-replenishment acquisitions using a low mechanical index. The authors emphasize the importance of linearizing ultrasound data according to the type and settings of the imaging equipment, as opposed to grey levels intensities directly extracted from the log-compressed images visible on the monitor. More importantly, they present a perfusion model accounting for the variety in blood flow velocity and direction, assuming a model accurately describing the distribution of transit times is known (e.g. log-normal distribution). The method achieves a better description of the S-shaped replenishment curves that can be observed.

In 2009, Quaia et al. [46] proposed a model reflecting the drag (related to flow) and diffusion (not related to flow) of microbubbles in blood, and accounting for the variety of blood velocities and directions. This variety is modeled as the sum of a variable number of piecewise linear replenishment curves. The model was validated through in vitro experiments using a dialysis cartridge with tubular capillaries, and in vivo experiments in the renal cortex of 12 healthy volunteers, separated in two age groups. While it achieved a significantly better fit than the exponential model using a Wilcoxon signed-rank test, whether the proposed model was using two, three, or four different tracts, the differences in the mean squared error remained extremely small and exhibited non-negligible overlap. Furthermore, while the authors report a significant difference in the initial replenishment slope among the two age groups using the proposed model, based a Mann-Whitney U-test, they do not report on the slope differences obtained using the exponential model, nor on the apparent concordance of the plateau values obtained using the two models.

2.2 Deconvolution methods

2.3 Compartmental models

Bibliography

[1] W F Armstrong, T M Mueller, E L Kinney, E G Tickner, J C Dillon, and H Feigenbaum. Assessment of myocardial perfusion abnormalities with contrast-enhanced two-dimensional echocardiography. *Circulation*, 66(1):166–173, July 1982. 26

[2] S Aronson, J G Wiencek, S B Feinstein, P A Heidenreich, J G Zaroff, R Walker, and M F Roizen. Assessment of renal blood flow with contrast ultrasonography. *Anesthesia & ...*, 76(5):964–970, May 1993. 28

[3] D M Band, R A Linton, T K O'Brien, M M Jonas, and N W Linton. The shape of indicator dilution curves used for cardiac output measurement in man. *The Journal of Physiology*, 498(1):225–229, January 1997. 31

[4] A Baur, A Stäbler, R Bartl, R Lamerz, J Scheidler, and M Reiser. MRI gadolinium enhancement of bone marrow: age-related changes in normals and in diffuse neoplastic infiltration. *Skeletal radiology*, 26(7):414–418, July 1997. 24

[5] H Bleeker, K Shung, and J Barnhart. On the application of ultrasonic contrast agents for blood flowmetry and assessment of cardiac perfusion. *Journal of ultrasound in medicine : official journal of the American Institute of Ultrasound in Medicine*, 9(8): 461–471, August 1990. 27

[6] Martin J K Blomley, Richard Coulden, Peter Dawson, Martti Kormano, Pamela Donlan, Cecile Bufkin, and Martin J Lipton. Liver Perfusion Studied with Ultrafast CT. *Journal of Computer Assisted Tomography*, 19(3):424–433, May 1995. 20, 21

[7] William Bommer, James Neef, Alexander Neumann, Lynn Weinert, Garrett Lee, Dean T Mason, and Anthony N DeMaria. Indicator-dilution curves obtained by photometric analysis of two-dimension echo-contrast studies. *American Journal of Cardiology*, 41(2):370, February 1978. 25

[8] R C Brasch, H J Weinmann, and G E Wesbey. Contrast-enhanced NMR imaging: animal studies using gadolinium-DTPA complex. *AJR. American journal of roentgenology*, 142(3):625–630, March 1984. 22

[9] P N Burns, S R Wilson, and D H Simpson. Pulse inversion imaging of liver blood flow: improved method for characterizing focal masses with microbubble contrast. *Investigative Radiology*, 35(1):58–71, January 2000. 33

[10] B D Butler and B A Hills. The lung as a filter for microbubbles. *Journal of applied physiology: respiratory, environmental and exercise physiology*, 47(3):537–543, September 1979. 24

[11] Anthony N DeMaria, William Bommer, Lily George, Alexander Neumann, Lynn Weinert, and Dean T Mason. Combined peripheral venous injection and cross-sectional echocardiography in the evaluation of cardiac disease. *American Journal of Cardiology*, 41(2):370, February 1978. 25

[12] C F Dietrich, Michalakis Averkiou, J-M Correas, N Lassau, E Leen, and F Piscaglia. An EFSUMB introduction into Dynamic Contrast-Enhanced Ultrasound (DCE-US) for quantification of tumour perfusion. In *Ultraschall in der Medizin (Stuttgart, Germany : 1980)*, pages 344–351. Innere Medizin 2, Caritas-Krankenhaus, Bad Mergentheim. Christoph.Dietrich@ckbm.de, © Georg Thieme Verlag KG, August 2012. 20

[13] P E Dugdale and K A Miles. Hepatic metastases: the value of quantitative assessment of contrast enhancement on computed tomography. *European journal of radiology*, 30 (3):206–213, June 1999. 21

[14] R Erlemann, M F Reiser, P E Peters, P Vasallo, B Nommensen, C R Kusnierz-Glaz, J Ritter, and A Roessner. Musculoskeletal neoplasms: static and dynamic Gd-DTPA–enhanced MR imaging. *Radiology*, 171(3):767–773, June 1989. 20, 23, 24

[15] Jens Eyding, Christos Krogias, Wilko Wilkening, Saskia Meves, Helmut Ermert, and Thomas Postert. Parameters of cerebral perfusion in phase-inversion harmonic imaging (PIHI) ultrasound examinations. *Ultrasound in Medicine & Biology*, 29(10):1379–1385, October 2003. 32

[16] S B Feinstein, F J Ten Cate, W Zwehl, K Ong, G Maurer, C Tei, P M Shah, S Meerbaum, and E Corday. Two-dimensional contrast echocardiography. I. In vitro development

and quantitative analysis of echo contrast agents. *Journal of the American College of Cardiology*, 3(1):14–20, January 1984. 26

[17] R Felix, W Schörner, M Laniado, H P Niendorf, C Claussen, W Fiegler, and U Speck. Brain tumors: MR imaging with gadolinium-DTPA. *Radiology*, 156(3):681–688, September 1985. 22

[18] Donald J Hagler, Abdul J Tajik, James B Seward, and Erik L Ritman. Videodensitometric Quantitation of Left-to-Right Shunts with Contrast Echocardiography. In *Contrast Echocardiography*, pages 298–303. Springer Netherlands, Dordrecht, 1982. 25

[19] W F Hamilton, John Walker Moore, J M Kinsman, and R G Spurling. STUDIES ON THE CIRCULATION. *American Journal of Physiology – Legacy Content*, 99(3):534–551, February 1932. 24

[20] P A Heidenreich, J G Wiencek, J G Zaroff, S Aronson, L J Segil, P V Harper, and S B Feinstein. In vitro calculation of flow by use of contrast ultrasonography. *Journal of the American Society of Echocardiography*, 6(1):51–61, January 1993. 27

[21] A J Hilson, M N Maisey, C B Brown, C S Ogg, and M S Bewick. Dynamic renal transplant imaging with Tc-99m DTPA (Sn) supplemented by a transplant perfusion index in the management of renal transplants. *Journal of nuclear medicine : official publication, Society of Nuclear Medicine*, 19(9):994–1000, September 1978. 20

[22] Sanjiv Kaul, Paul Kelly, Jonathan D Oliner, William P Glasheen, Mark W Keller, and Denny D Watson. Assessment of regional myocardial blood flow with myocardial contrast two-dimensional echocardiography. *Journal of the American College of Cardiology*, 13(2):468–482, February 1989. 30

[23] Grete Mørk Kindberg, Helge Tolleshaug, Norbert Roos, and Tore Skotland. Hepatic clearance of Sonazoid perfluorobutane microbubbles by Kupffer cells does not reduce the ability of liver to phagocytose or degrade albumin microspheres. *Cell and tissue research*, 312(1):49–54, 2003. 24

[24] E Klotz and M König. Perfusion measurements of the brain: using dynamic CT for the quantitative assessment of cerebral ischemia in acute stroke. *European journal of radiology*, 30(3):170–184, June 1999. 22

[25] M Koenig, E Klotz, B Luka, D J Venderink, J F Spittler, and L Heuser. Perfusion CT of the brain: diagnostic approach for early detection of ischemic stroke. *Radiology*, 209 (1):85–93, October 1998. 20, 22

[26] Martin Krix, Fabian Kiessling, Nabeel Farhan, Kerstin Schmidt, Johannes Hoffend, and Stefan Delorme. A multivessel model describing replenishment kinetics of ultrasound contrast agent for quantification of tissue perfusion. *Ultrasound in Medicine & Biology*, 29(10):1421–1430, October 2003. 33

[27] Martin Krix, Fabian Kiessling, Silvia Vosseler, Isabel Kiessling, Martin Le-Huu, Norbert E Fusenig, and Stefan Delorme. Comparison of intermittent-bolus contrast imaging with conventional power Doppler sonography: quantification of tumour perfusion in small animals. *Ultrasound in Medicine & Biology*, 29(8):1093–1103, August 2003. 34

[28] Christos Krogias, Thomas Postert, Saskia Meves, Wilko Wilkening, Horst Przuntek, and Jens Eyding. Semiquantitative analysis of ultrasonic cerebral perfusion imaging. *Ultrasound in Medicine & Biology*, 31(8):1007–1012, August 2005. 32

[29] Marios Lampaskis and Michalakis Averkiou. Investigation of the relationship of nonlinear backscattered ultrasound intensity with microbubble concentration at low MI. *Ultrasound in Medicine & Biology*, 36(2):306–312, February 2010. 24

[30] R A F Linton, N W F Linton, and D M Band. A new method of analysing indicator dilution curves. *Cardiovascular research*, 30(6):930–938, December 1995. 31

[31] H Masugata, B Peters, S Lafitte, G M Strachan, K Ohmori, and A N DeMaria. Quantitative assessment of myocardial perfusion during graded coronary stenosis by real-time myocardial contrast echo refilling curves. *Journal of the American College of Cardiology*, 37(1):262–269, January 2001. 33

[32] R S Meltzer, J Roelandt, O L Bastiaans, L Piérard, P W Serruys, and C T Lancée. Video-densitometric processing of contrast two-dimensional echocardiographic data. *Ultrasound in Medicine & Biology*, 8(5):509–514, 1982. 25

[33] K A Miles. Measurement of tissue perfusion by dynamic computed tomography. *The British journal of radiology*, 64(761):409–412, May 1991. 20, 21

[34] K A Miles. Functional computed tomography in oncology. *European Journal of Cancer*, 38(16):2079–2084, November 2002. 21

[35] K A Miles, M Hayball, and A K Dixon. Colour perfusion imaging: a new application of computed tomography. *The Lancet*, 337(8742):643–645, March 1991. 20, 21

[36] K A Miles, M P Hayball, and A K Dixon. Functional images of hepatic perfusion obtained with dynamic CT. *Radiology*, 188(2):405–411, August 1993. 20, 21

[37] K A Miles, M P Hayball, and A K Dixon. Measurement of human pancreatic perfusion using dynamic computed tomography with perfusion imaging. *The British journal of radiology*, 68(809):471–475, May 1995. 21

[38] J V Nally, H S Clarke, J P Windham, G P Grecos, M L Gross, and W J Potvin. Technetium-99m DTPA renal flow studies in Goldblatt hypertension. *Journal of nuclear medicine : official publication, Society of Nuclear Medicine*, 26(8):917–924, August 1985. 20, 21

[39] David Norman, Edwin A Stevens, S Douglas Wing, Victor Levin, and Thomas H Newton. Quantitative Aspects of Contrast Enhancement in Cranial Computed Tomography. *Radiology*, 129(3):683–688, December 1978. 20

[40] A M Peters, J Brown, G G Hartnell, M J Myers, C Haskell, and J P Lavender. Non-invasive measurement of renal blood flow with 99mTc DTPA: comparison with radiolabelled microspheres. *Cardiovascular research*, 21(11):830–834, November 1987. 20, 21

[41] A M Peters, R D GUNASEKERA, B L HENDERSON, J Brown, J P Lavender, M DE SOUZA, J M ASH, and D L GILDAY. Noninvasive measurement of blood flow and extraction fraction. *Nuclear Medicine Communications*, 8(10):823–837, October 1987. 20, 21

[42] Holger Pettersson, N Ackerman, J Kaude, R E Googe, A A Mancuso, K N Scott, R H Hackett, D A Hager, and S Caballero. Gadolinium-DTPA Enhancement of Experimental Soft Tissue Carcinoma and Hemorrhage in Magnetic Resonance Imaging. *Acta ...*, 28(1):75–78, January 1987. 20, 23

[43] T Postert, P Hoppe, J Federlein, S Helbeck, H Ermert, H Przuntek, T Büttner, and W Wilkening. Contrast agent specific imaging modes for the ultrasonic assessment of parenchymal cerebral echo contrast enhancement. *Journal of Cerebral Blood Flow & Metabolism*, 20(12):1709–1716, December 2000. 31

[44] T C Potdevin, J B Fowlkes, A P Moskalik, and P L Carson. Analysis of refill curve shape in ultrasound contrast agent studies. *Medical physics*, 31(3):623–632, March 2004. 34

[45] Titaina C U Potdevin, J Brian Fowlkes, Aaron P Moskalik, and Paul L Carson. Refill model of rabbit kidney vasculature. *Ultrasound in Medicine & Biology*, 32(9):1331–1338, September 2006. 34

[46] Emilio Quaia, Aldo Nocentini, and Lucio Torelli. Assessment of a new mathematical model for the computation of numerical parameters related to renal cortical blood flow and fractional blood volume by contrast-enhanced ultrasound. *Ultrasound in Medicine & Biology*, 35(4):616–627, April 2009. 35

[47] D Revel, R C Brasch, H Paajanen, W Rosenau, W Grodd, B Engelstad, P Fox, and J Winkelhake. Gd-DTPA contrast enhancement and tissue differentiation in MR imaging of experimental breast carcinoma. *Radiology*, 158(2):319–323, February 1986. 23

[48] T Schlosser, C Pohl, C Veltmann, S Lohmaier, J Goenechea, A Ehlgen, J Köster, D Bimmel, S Kuntz-Hehner, H Becher, and K Tiemann. Feasibility of the flash-replenishment

concept in renal tissue: which parameters affect the assessment of the contrast replenishment? *Ultrasound in Medicine & Biology*, 27(7):937–944, July 2001. 33

[49] K Q Schwarz, G P Bezante, X Chen, J G Mottley, and R Schlief. Volumetric arterial flow quantification using echo contrast. An in vitro comparison of three ultrasonic intensity methods: radio frequency, video and Doppler. *Ultrasound in Medicine & Biology*, 19 (6):447–460, 1993. 29

[50] D H Simpson and P N Burns. Pulse inversion Doppler: a new method for detecting nonlinear echoes from microbubble contrast agents. *Ultrasonics Symposium*, 1997. 33

[51] G N Stewart. Researches on the Circulation Time and on the Influences which affect it. *The Journal of Physiology*, 22(3):159–183, November 1897. 19, 24

[52] T Stolnikow. *Die Aichung des Blutetromes in der Aorta des Hundes*. Arch f Anat u Physiol, 1886. 19

[53] R W Stow and P S Hetzel. An empirical formula for indicator-dilution curves as obtained in human beings. *Journal of applied physiology*, 7(2):161–167, September 1954. 31

[54] Ukihide Tateishi, Hiroshi Nishihara, Satoshi Watanabe, Toshiaki Morikawa, Kazuhiro Abe, and Kazuo Miyasaka. Tumor Angiogenesis and Dynamic CT in Lung Adenocarcinoma: Radiologic–Pathologic Correlation. *Journal of Computer Assisted Tomography*, 25(1):23–27, January 2001. 21

[55] C Tei, T Sakamaki, P M Shah, S Meerbaum, K Shimoura, S Kondo, and E Corday. Myocardial contrast echocardiography: a reproducible technique of myocardial opacification for identifying regional perfusion deficits. *Circulation*, 67(3):585–593, March 1983. 26

[56] F J Ten Cate, J K Drury, S Meerbaum, J Noordsy, S Feinstein, P M Shah, and E Corday. Myocardial contrast two-dimensional echocardiography: experimental examination at different coronary flow levels. *Journal of the American College of Cardiology*, 3(5): 1219–1226, May 1984. 26

[57] F J Ten Cate, J H Cornel, P W Serruys, W B Vletter, J Roelandt, and W H Mittertreiner. Quantitative assessment of myocardial blood flow by contrast two-dimensional echocardiography: initial clinical observations. *American journal of physiologic imaging*, 2(2):56–60, 1987. 26

[58] K Tiemann and H Becher. *Real-time assessment of tissue perfusion following bubble destruction at low emission power-First experimental results using power pulse inversion* .... JOURNAL OF ..., 2000. 33

[59] K Tiemann, T Schlosser, C Pohl, D Bimmel, G Wietasch, A Hoeft, J Likungu, C Vahlhaus, S Kuntz, N C Nanda, H Becher, and B Lüderitz. Are microbubbles free flowing tracers through the Myocardium? Comparison of indicator-dilution curves obtained from dye dilution and echo contrast using harmonic power Doppler imaging. *Echocardiography (Mount Kisco, N.Y.)*, 17(1):17–27, January 2000. 31

[60] Klaus Tiemann, Harald Becher, Dieter Bimmel, Reinhard Schlief, and Navin C Nanda. Stimulated Acoustic Emission Nonbackscatter Contrast Effect of Microbubbles Seen with Harmonic Power Doppler Imaging. *Echocardiography (Mount Kisco, N.Y.)*, 14(1): 65–70, January 1997. 31

[61] Klaus Tiemann, Stefan Lohmeier, Stefanie Kuntz, Jörg Köster, Christoph Pohl, Peter Burns, Thomas R, Navin C Nanda, Berndt Lüderitz, and Harald Becher. Real-Time Contrast Echo Assessment of Myocardial Perfusion at Low Emission Power: First Experimental and Clinical Results Using Power Pulse Inversion Imaging. *Echocardiography (Mount Kisco, N.Y.)*, 16(8):799–809, November 1999. 33

[62] R Tigerstedt. *Bestimmung der von dem linken Herzen herausgetriebenen Blutmenge*. Skand. Arch. f. Physiol, 1891. 19

[63] Yoshito Tsushima, Martin J K Blomley, Shoichi Kusano, and Keigo Endo. The Portal Component of Hepatic Perfusion Measured by Dynamic CT (An Indicator of Hepatic Parenchymal Damage). *Digestive Diseases and Sciences*, 44(8):1632–1638, 1999. 22

[64] Byron F Vandenberg, Robert Kieso, Karen Fox-Eastham, William Chilian, and Richard E Kerber. Quantitation of myocardial perfusion by contrast echocardiography: Analysis of contrast gray level appearance variables and intracyclic variability. *Journal of the American College of Cardiology*, 13(1):200–206, January 1989. 26

[65] K L Verstraete, Y De Deene, H Roels, A Dierick, D Uyttendaele, and M Kunnen. Benign and malignant musculoskeletal lesions: dynamic contrast-enhanced MR imaging–parametric "first-pass" images depict tissue vascularization and perfusion. *Radiology*, 192(3):835–843, September 1994. 24

[66] C Vierordt. Die Erscheinungen und Gesetze der Stromgeschwindigkeiten des Blutes: Nach Versuchen, 1858. 19

[67] A W Volkmann. *Die Hämodynamik*. 1850. 19

[68] Kevin Wei, Ananda R Jayaweera, Soroosh Firoozan, Andre Linka, Danny M Skyba, and Sanjiv Kaul. Quantification of Myocardial Blood Flow With Ultrasound-Induced Destruction of Microbubbles Administered as a Constant Venous Infusion. *Circulation*, 97(5):473–483, February 1998. 33

[69] Kevin Wei, Elizabeth Le, Jian-Ping Bin, Matthew Coggins, Jerrel Thorpe, and Sanjiv Kaul. Quantification of renal blood flow with contrast-enhanced ultrasound. *Journal of the American College of Cardiology*, 37(4):1135–1140, March 2001. 33

[70] H J Weinmann, R C Brasch, W R Press, and G E Wesbey. Characteristics of gadolinium-DTPA complex: a potential NMR contrast agent. *AJR. American journal of roentgenology*, 142(3):619–624, March 1984. 22

[71] G E Wesbey, C B Higgins, M T McNamara, B L Engelstad, M J Lipton, R Sievers, R L Ehman, J Lovin, and R C Brasch. Effect of gadolinium-DTPA on the magnetic relaxation times of normal and infarcted myocardium. *Radiology*, 153(1):165–169, October 1984. 22

[72] J G Wiencek, S B Feinstein, R Walker, and S Aronson. Pitfalls in quantitative contrast echocardiography: the steps to quantitation of perfusion. *Journal of the American Society of Echocardiography*, 6(4):395–416, July 1993. 29, 30

[73] W Wijns, P W Serruys, J H Reiber, M van den Brand, M L Simoons, C J Kooijman, K Balakumaran, and P G Hugenholtz. Quantitative angiography of the left anterior descending coronary artery: correlations with pressure gradient and results of exercise thallium scintigraphy. *Circulation*, 71(2):273–279, February 1985. 27

[74] M E Wise. The geometry of log-normal and related distributions and an application to tracer-dilution curves. *Statistica Neerlandica*, 20(1):119–142, March 1966. 31

[75] Kyosuke Yanagisawa, Fuminori Moriyasu, Takeo Miyahara, Miyata Yuki, and Hiroko Iijima. Phagocytosis of ultrasound contrast agent microbubbles by Kupffer cells. *Ultrasound in Medicine & Biology*, 33(2):318–325, February 2007. 24

[76] M Zhang and M Kono. Solitary pulmonary nodules: evaluation of blood flow patterns with dynamic CT. *Radiology*, 205(2):471–478, November 1997. 21

Chapter 3

Quantification of tumor perfusion using DCE-US: impact of mathematical modeling

3.1 Abstract

Dynamic Contrast Enhanced Ultrasound has been proposed to monitor tumor therapy, in complement to volume measurements. To assess the variability of perfusion parameters in ideal conditions, four consecutive test-retest studies were acquired in a tumor model of mouse, using controlled injections. The impact of mathematical modeling on parameter variability was then investigated. Coefficients of variation (CV) of tissue blood volume (BV) and tissue blood flow (BF) based-parameters were estimated inside 32 sub-regions of the tumors, comparing the log-normal (LN) model with a one-compartment model fed by an arterial input function (AIF) and improved by the introduction of a time delay parameter. Relative perfusion parameters were also estimated by normalization of the LN parameters and normalization of the one-compartment parameters estimated with the AIF, using a reference tissue (RT) region. A direct estimation (rRTd) of relative parameters based on the one-compartment model without using the AIF was also obtained by using the kinetics inside the RT region. Results on test-retest studies show that absolute regional parameters

have high CV, whatever the approach, with median values of about 30% for BV, and 40% for BF. The positive impact of normalization was established, showing a coherent estimation of relative parameters, with reduced CV (about 20% for BV and 30% for BF using the rRTd approach). These values were significantly lower ($p < 0.05$) when compared to CV of absolute parameters. The rRTd approach provided the smallest CV and should be preferred for estimating relative perfusion parameters.

3.2 Introduction

Reliable quantification of tumor perfusion is a challenging objective in order to establish cancer diagnosis and to monitor therapy. Tumor perfusion can be assessed through various imaging modalities, including PET, Dynamic Contrast Enhanced (DCE) MR, CT and ultrasound (DCE-US).

Compared to DCE-MRI, DCE-CT and PET, the main advantages of DCE-US are its real-time, non-ionizing, and cost-effective characteristics. Moreover, as micro-bubbles do not diffuse in the extra-vascular space, DCE-US studies reflect only the tissue vasculature. Different acquisition protocols are available including bolus and destruction-replenishment during infusion [24]. The present work focuses on bolus injections, since this acquisition mode is the most widely used [2].

It is currently recommended for bolus DCE-US studies to estimate semi-quantitative parameters using explicit models, such as the Log-Normal model [17]. However, it was shown that these semi-quantitative parameters were sensitive to various factors [18]: scanner-related (e.g. frequency, mechanical index, dynamic range, focal length), patient-related (e.g. blood pressure, tissue motion, physiological interaction), and bubble-related (e.g. bubble type, concentration, preparation, injection) factors. The quantification of bolus DCE-US studies thus remains a major challenge.

In an attempt to make quantification of tissue perfusion less sensitive to external factors, quantitative approaches based on indicator dilution theory and commonly used for PET, DCE-MRI or DCE-CT exams [14, 19, 23] could be applied to DCE-US data. These methods estimate tissue blood volume and tissue blood flow parameters by performing a specific de-

convolution of the tissue time-intensity curve inside the tumor by an Arterial Input Function (AIF) measured in the imaging plane. Similarly to what was done in above cited imaging modalities, a compartmental approach was recently proposed for DCE-US [4]. Precisely, a one-compartment model was proposed since the contrast agent remains in the blood. This approach defines a set of admissible curves for the transfer function (mono-exponential functions), and the estimation of parameters is then regularized intrinsically. It can thus be distinguished from blind deconvolutions, as recently proposed in DCE-US [5, 10]. Indeed, these approaches require establishing strong constraints on the transfer functions, due to their large number of unknown parameters.

The present study aimed at comparing different modeling approaches and at studying the reproducibility of perfusion parameters in test-retest measurements on a mouse tumor model, acquired using controlled injections [3]. Three absolute modeling approaches including a Log-Normal model and a one-compartment model without and with a time delay were first compared. In a second time, relative perfusion parameters were defined by normalizing the values obtained in the tumor with values obtained in a reference tissue region, and five relative derived models were studied.

3.3 Materials

3.3.1 Animals

Murine Lewis Lung Carcinoma (3LL) were used. Tumor fragments (20-40 mm^3) were implanted subcutaneously 20 days prior to the experiment in the right flank of four Balb/C mice. All experiments were conducted in accordance with the institutional guidelines and the recommendations for the care and use of laboratory animals.

Prior to imaging, animals were individually placed in an induction chamber, where anesthesia was induced with 4% isoflurane in air with delivery rate of 1 L/min. Anesthesia was maintained with 2% isoflurane in air delivered by a face mask with the same delivery rate. The temperature of the animal was regulated using a thermostatic heating plate (Minerve, Esternay, France). Each mouse was secured in position with surgical tape so that the oper-

ator could not inadvertently reposition it during the procedure.

3.3.2 Image acquisition

Dynamic contrast-enhanced US sequences were acquired using a 15L8W transducer and a Sequoia 512 US system (Acuson, Siemens, Mountain View, CA, USA) with constant mechanical index (0.1), dynamic range (80 dB), and time gain compensation settings. The imaging plane was selected as the largest cross-section of the tumor and the probe was fixed to a support in the selected position.

A bolus of 50 µL of SonoVue (Bracco Suisse SA, Geneva, Switzerland) diluted to 20% was injected at a rate of 4.5 mL/min using a controlled injection system to improve acquisition reproducibility [3]. This diluted concentration was proposed to reduce attenuation artifacts. Each acquisition consisted of a 4 minute dual-mode recording, including B-Mode and Contrast Pulse Sequencing (CPS) images, using a frame rate of 3 Hz during the first 30 seconds (including the wash-in phase and the beginning of the wash-out phase), and 1 Hz for the remaining time. Four consecutive (test-retest) studies were acquired for each mouse without any modification in the setup. Fifteen minute breaks were observed between acquisitions to ensure the destruction of all circulating micro-bubbles.

3.3.3 Data pre-processing

Linear echo-power kinetics were extracted from log-compressed video data using a validated home-made software calibrated using dose-ranging data [16]. Both probe and animal motion were assumed negligible for the selected sequences.

Tumors were segmented on the B-mode acquisition and necrotic zones were excluded as previously described [3]. In order to further reveal spatial heterogeneity inside the tumor, a regional analysis of the tumor area was performed. Dividing the non-necrotic tumor region into 32 sub-regions according to 4 radial layers and 8 angular sectors (Figure 3-1) provided a good compromise between showing heterogeneity while preserving the signal to noise ratio of the time-intensity curves and the spatial matching of the sub-regions between the four test-retest studies.

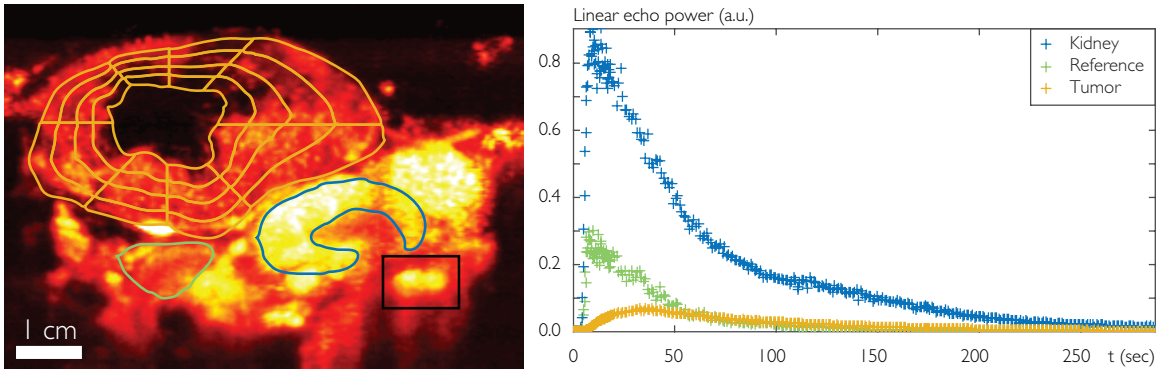

Figure 3-1: Illustration of the data pre-processing steps. Left: The contours of the tumor and its necrotic core have been overlaid on a contrast enhanced image (in ochre color). The perfused tumor area was divided into 4 radial layers and 8 angular sectors. A reference tissue region (in green color) and a renal cortex region (in blue color) were also delineated. Right: Mean kinetics associated with the non-necrotic part of the tumor, the reference tissue, and the renal cortex.

3.4 Methods

3.4.1 Quantification of tumor perfusion

Table 3.1 summarizes the main features of the eight methods tested, three absolute and five relative, for tumor perfusion quantification. Some methods require the definition of an arterial region in order to estimate the AIF, its estimation is presented in section 3.4.1. Relative quantification methods require the selection of a reference tissue region (labeled with subscript R). This region was segmented in order to define a homogeneous area, while being large enough in order to reduce noise influence on the subsequent analysis (Figure 3-1).

For all methods, quantitative parameters were derived by the minimization of the root-mean-square error between the time-intensity curve inside the tumor, $C_T(t)$, and the corresponding fitted curve, using an interior-point algorithm (MATLAB, MathWorks, Natick, MA, USA). To make the comparison between models easier, we focused on volume-based, flow-based, and time delays parameters.

Acronym	Model Name	Input data AIF/RT	Eq.	Parameters
aLN	Log-Normal	No/No	(3.1)	AUC, WIR, Δ
aAIF	One-Compartment	Yes/No	(3.2)	V, F
aAIFd	One-Compartment with delay	Yes/No	(3.2)	V, F, d
rLN	Relative Log-Normal	No/Yes	(3.1,5.5)	$rAUC, rWIR, D$
rAIF	Relative One-Compartment	Yes/Yes	(3.2,3.4)	rV_{AIF}, rF_{AIF}
rAIFd	Relative One-Compartment with delay	Yes/Yes	(3.2,3.4)	$rV_{AIF}, rF_{AIF}, D_{AIF}$
rRT	Relative Reference Tissue	No/Yes	(3.5,3.6)	rV_{RT}, rF_{RT}
rRTd	Relative Reference Tissue with delay	No/Yes	(3.5,3.6)	rV_{RT}, rF_{RT}, D_{RT}

Table 3.1: Synthesis of the different models tested. The first three models propose absolute quantification. The last five models propose relative quantification.

Absolute Log-normal model: aLN [17].

The kinetics $C_T(t)$ is fitted according to the equation (3.1):

$$\begin{aligned} C_T(t) &= \frac{AUC_T}{\sqrt{2\pi}\sigma_T(t-\Delta_T)} \exp\left(-\frac{[\ln(t-\Delta_T)-\mu_T]^2}{2{\sigma_T}^2}\right) \text{ if } t > \Delta_T, \\ &= 0 \text{ otherwise,} \end{aligned} \tag{3.1}$$

where AUC_T is the area under the C_T curve, μ_T and σ_T are the expectation and standard deviation of the distribution $C_T(\tau)/AUC_T$ when substituting $\ln(t-\Delta_T)$ with τ, and Δ_T represents the time shift between the start of the acquisition and the arrival of the contrast agent in the tumor. As the area under the curve AUC_T is related to the tissue blood volume [20] and the wash-in rate WIR_T (derived from AUC_T, μ_T and σ_T) is related to the tissue blood flow [2], these two parameters were estimated in addition to Δ_T in the remaining analysis.

One-Compartment model with an Arterial Input Function: aAIF and aAIFd

[7]. The mathematical expression of $C_T(t)$ is given by equation (3.2):

$$\begin{aligned} C_T(t) &= F_T \int_0^{t-d_T} C_A(\tau) \exp^{-\frac{F_T}{V_T}(t-d_T-\tau)} \mathrm{d}\tau \quad \text{if } t \geq d_T, \\ &= 0 \text{ otherwise,} \end{aligned} \tag{3.2}$$

where $C_A(t)$ is the kinetics inside the feeding artery (the AIF), V_T the tissue blood volume (in %), F_T the tissue blood flow (in s^{-1}), and d_T (in s) the time-delay of the contrast agent from the feeding artery to the tumor. When it is neglected ($d_T = 0$), the model is noted **aAIF**. When it is estimated in addition to V_T and F_T, the model is noted **aAIFd**.

To estimate the AIF, a bounding box surrounding arterial vessels was first defined according to anatomical considerations and high values of enhancement (see Figure 3-1). Peak Enhancement (PE) and Time To Peak (TTP) parametric maps were then computed for each pixel of the bounding box. The maximal value of PE (PE_{max}) and the minimal value of TTP (TTP_{min}) were extracted. Pixels verifying $PE/PE_{max} \geq rPE^*$ and $TTP - TTP_{min} \leq \Delta TTP^*$ were considered as part of the artery region (Figure 3-2), where rPE^* and ΔTTP^* are empirically chosen cut-off values, equal to 50% and 3 s, unless specified differently. The AIF, $C_A(t)$, was computed as the geometric mean of the kinetics inside the artery region and modeled using the LN model (3.1).

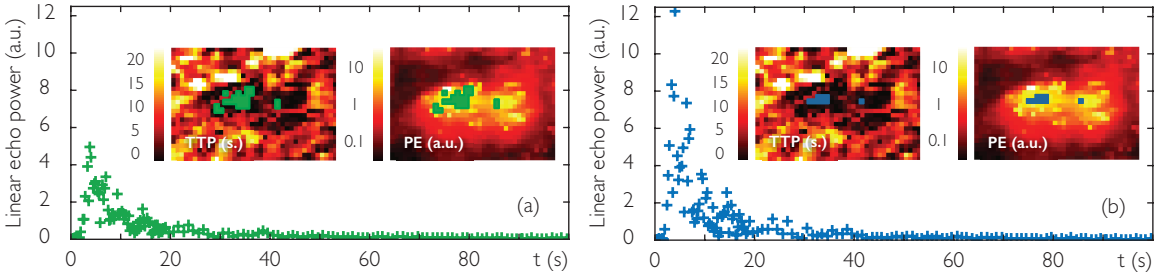

Figure 3-2: Automated detection of the AIF: parametric maps TTP and PE inside the artery region; segmentation results and associated AIF with: (a) $rPE^* = 50\%$ and $\Delta TTP^* = 3$ s (in green color); (b) $rPE^* = 70\%$ and $\Delta TTP^* = 2.5$ s (in blue color).

Relative Log-Normal model: rLN.

This model estimates three relative parameters: the relative area under the curve $rAUC$, the relative wash-in rate $rWIR$, and the time delay between the arrival of the contrast in the tumor and the reference tissue D_{T-R} according to equation (5.5):

$$rAUC = \frac{AUC_T}{AUC_R}, \quad rWIR = \frac{WIR_T}{WIR_R}, \quad \text{and} \quad D_{LN}^{T-R} = \Delta_T - \Delta_R, \tag{3.3}$$

where $(AUC_T,\ WIR_T,\ \Delta_T)$ and $(AUC_R,\ WIR_R,\ \Delta_R)$ are the absolute LN parameters estimated in the tumor and in the reference tissue respectively using equation (3.1).

Relative One-Compartment model with an Arterial Input Function: rAIF and rAIFd.

This model estimates three parameters: the relative blood volume rV_{AIF}, the relative blood flow rF_{AIF} and the time delay between the arrival of the contrast in the tumor and the reference tissue D_{AIF}^{T-R} according to equation (3.4):

$$rV_{AIF} = \frac{V_T}{V_R}, \quad rF_{AIF} = \frac{F_T}{F_R}, \quad \text{and} \quad D_{AIF}^{T-R} = d_T - d_R, \tag{3.4}$$

where (V_T, F_T, d_T) and (V_R, F_R, d_R) are the perfusion parameters estimated in the tumor and in the reference tissue respectively using the AIF according to equation (3.2). This method is referred to as **rAIF** when D_{AIF}^{T-R} is set to zero and **rAIFd** otherwise.

Relative One-Compartment model using the Reference Tissue kinetics: rRT and rRTd

[15, 25]. This model estimates three parameters: the relative blood volume rV_{RT}, the relative blood flow rF_{RT} and the time delay between the arrival of the contrast in the tumor and the reference tissue D_{RT}^{T-R}, the subscript $_{RT}$ being used for distinguishing this approach from the previous one (section 3.4.1). Assuming that the tumor and the reference region have a common AIF, the kinetics $C_R(t)$ and $C_T(t)$ can be described by equation (3.2). When replacing $C_A(t)$ by its expression as a function of $C_R(t)$ in equation (3.2), $C_T(t)$ can then be described by equation (5):

$$\begin{aligned} C_T(t) &= rF_{RT}\Big[C_R\left(t - D_{RT}^{T-R}\right) \\ &\qquad + (k_R - k_T)\int_{d_R}^{t-D_{RT}^{T-R}} C_R(\tau)\, e^{-k_T\left(t-D_{RT}^{T-R}-\tau\right)} \mathrm{d}\tau\Big] \quad \text{if } t \geq d_T, \\ &= 0 \text{ otherwise,} \end{aligned} \tag{3.5}$$

where $k_R = F_R/V_R$ and $k_T = F_T/V_T$. The parameter k_R was chosen as the mean value of the k_R values estimated with the relative AIF approach (**rAIFd**) and was set to 0.15. The parameters rF_{RT}, k_T andD_{RT}^{T-R} were estimated by solving equation (3.5). The parameter rV_{RT} was then

deduced using equation (3.6):

$$rV_{RT} = \frac{V_T}{V_R} = \frac{F_T}{k_T}\frac{k_R}{F_R} = rF_{RT}\frac{k_R}{k_T}. \tag{3.6}$$

The method is referred to as **rRT** when D_{RT}^{T-R} is set to zero and **rRTd** otherwise.

3.4.2 Data analysis

For each model, the quantitative assessment of the fit was achieved using the normalized root mean square error ($NRMSE$), and the fraction of information that is modeled (FMI), as defined in [1]. The $NRMSE$ was defined by:

$$NRMSE = \frac{\sqrt{\frac{1}{nt}\sum_{t=1}^{nt}\left(C_{fit}(t) - C(t)\right)^2}}{max_t(C(t)) - min_t(C(t))}, \tag{3.7}$$

where C and C_{fit} are the observed and fitted kinetics and nt is the total number of frames. A good fit corresponds to $NRMSE$ close to 0 and FMI close to 100%. For each sub-region, results for which $FMI < 90\%$ were judged as poor quality fits.

In order to assess the reproducibility of the parameters θ^{hl} of the mouse m_l (l from 1 to 4) in the sub-region s_h (h from 1 to 32), coefficients of variation CV^{hl} were estimated using the four test-retest studies, as follows:

$$CV^{hl} = \frac{\sqrt{\frac{1}{4}\sum_{k=1}^{4}(\theta^{hl}(k) - \mu^{hl})^2}}{\mu^{hl}}, \text{where } \mu^{hl} = \frac{1}{4}\sum_{k=1}^{4}\theta^{hl}(k), \tag{3.8}$$

$\theta^{hl}(k)$ being the parameter θ^{hl} estimated for the kth test-retest study (with k from 1 to 4). As parameters $\theta^{hl}(k)$ corresponding to poor quality fits were removed, missing values were replaced using multivariate imputation according to the R package {mice}, 'Multivariate Imputation by Chained Equations' [21], in order to compute CV^{hl} using four values systematically.

Statistical tests were performed to compare goodness of fit criteria and coefficients of variation between the different models, using the R package {coin}, 'Conditional Inference Procedures in a Permutation Test Framework' [9]. They were considered as significant when

Model	All data		$FMI > 90\%$		
	$NRMSE$	FMI	$NRMSE$	FMI	N
aLN	5.75 [4.70-7.41]	99.4 [98.5-99.8]	5.63 [4.62-7.00]	99.4 [98.8-99.8]	28
aAIF	9.95*† [6.03-24.2]	94.7*† [45.2-98.3]	6.72° [5.12-9.20]	97.8° [95.5-98.9]	212
aAIFd	6.21 [4.71-8.43]	98.7* [97.3-99.4]	6.04 [4.66-8.20]	98.8* [97.6-99.4]	19
rRT	7.72*‡ [5.83-9.85]	97.6*‡ [94.9-98.7]	7.45*‡ [5.71-9.34]	97.8*‡ [95.6-98.8]	56
rRTd	6.32 [4.91-8.21]	98.7* [97.2-99.4]	6.18 [4.85-8.00]	98.8* [97.6-99.4]	19

Table 3.2: Median [first-third quartiles] values of $NMRSE$ and FMI (in %) obtained for the different models. N is the number of sub-regions where $FMI < 90\%$. Significant differences between **aLN** and any other model are indicated by *. In addition, significant differences between **aAIF** (resp. **rRT**) and **aAIFd** (resp. **rRTd)** are indicated by † (resp. ‡). The symbol $^{\circ}$ indicates that comparisons were not reported due to the high number of missing data.

p values were less than 0.05. As all the tests were conducted on paired data, when goodness of fit criteria were removed (due to poor quality fits), they were replaced with imputed data. The non-parametric Friedman test with post-hoc analysis (Tukey's HSD test) was chosen for dealing with multiple comparisons.

3.5 Results

3.5.1 Model comparison through quality of fit criteria

Table 3.2 shows the quartile values of the quality of fit criteria ($NRMSE$ and FMI), which are computed for the 512 ($4 \times 4 \times 32$) tumor sub-regions for the five models: **aLN**, **aAIF**, **aAIFd**, **rRT**, and **rRTd**. Since the $NMRSE$ and FMI criteria obtained by the three relative methods **rLN**, **rAIF** and **rAIFd** are identical to those obtained by **aLN**, **aAIF** and **aAIFd**, these results are not reported in Table 3.2. Additionally, quartile values are provided for the N sub-regions verifying $FMI > 90\%$. Due to the large portion of missing data for the **aAIF** model when considering only good fits (the number of excluded regions, N, being equal to 212), results of hypothesis testing were not presented for that specific case. The **aLN** model shows slightly better quality criteria than the other models (these differences are significant for FMI in all cases, and significant for $NRMSE$ in case of **aAIF** and **rRT** models). The introduction of the time delay parameter (**aAIFd**, **rAIFd** and **rRTd** models)

significantly improved the modeling quality, according to both criteria. Furthermore, the number of cases for which $FMI < 90\%$ was largely reduced when taking into account the time delays. For these reasons, results obtained without time delays (**aAIF**, **rAIF** and **rRT**) were not further reported.

3.5.2 Model comparison through coefficients of variation

All mean values and standard deviations of the perfusion parameters are given for each mouse in Appendix, in Table 3.4. Figure 3-3 illustrates for one specific mouse (m_1) the comparison between the parameters estimated by the different models. It shows a high correlation between the volume-based parameters: AUC, $rAUC$, V, rV_{AIF}, and rV_{RT} as well as a high correlation between the flow-based parameters: WIR, $rWIR$, F, rF_{AIF}, and rF_{RT}. This figure shows also that there is a large range of values for each parameter within one tumor, demonstrating that perfusion parameters inside the different sub-regions of the tumor are far from being similar. Finally, it proves that the slopes may be quite different from one study to another, and that the use of relative parameters contributes to largely reduce the differences between the test-retest studies, the estimation of rF_{AIF} being less robust than the estimation of $rWIR$ or rF_{RT} for this specific example. Table 3.3 illustrates the influence of the AIF choice on the estimation of volume, flow, and time delay parameters. On this specific exam, two AIF were generated, the first one (AIF_1) with thresholds $rPE^* = 50\%$ and $\Delta TTP^* = 3$ s, the second one (AIF_2) with thresholds $rPE^* = 70\%$ and $\Delta TTP^* = 2.5$ s (as shown in Figure 3-2). The variations were very large for V and F parameters, while they remained moderate for rF_{AIF} and time delays, and very low for rV_{AIF}.

	V (%)	rV_{AIF}(%)	F (10^{-3} s^{-1})	rF_{AIF} (%)	d_T (s)	D_{AIF}^{T-R} (s)
AIF_1	8.02 ± 3.89	84.5 ± 40.9	6.54 ± 5.37	8.83 ± 7.24	2.4 ± 3.4	1.4 ± 3.4
AIF_2	4.65 ± 2.25	85.2 ± 41.3	3.20 ± 2.61	10.1 ± 8.21	2.0 ± 3.3	1.6 ± 3.3

Table 3.3: Mean ± standard deviation of the parameters estimated with the **aAIFd** and **rAIFd** models, using two different sets of cut-offs to generate the AIF functions.

Finally, Figure 4-2 shows the distributions of the coefficients of variation of volume-based and flow-based parameters, computed according to equation (3.8). Relative volume

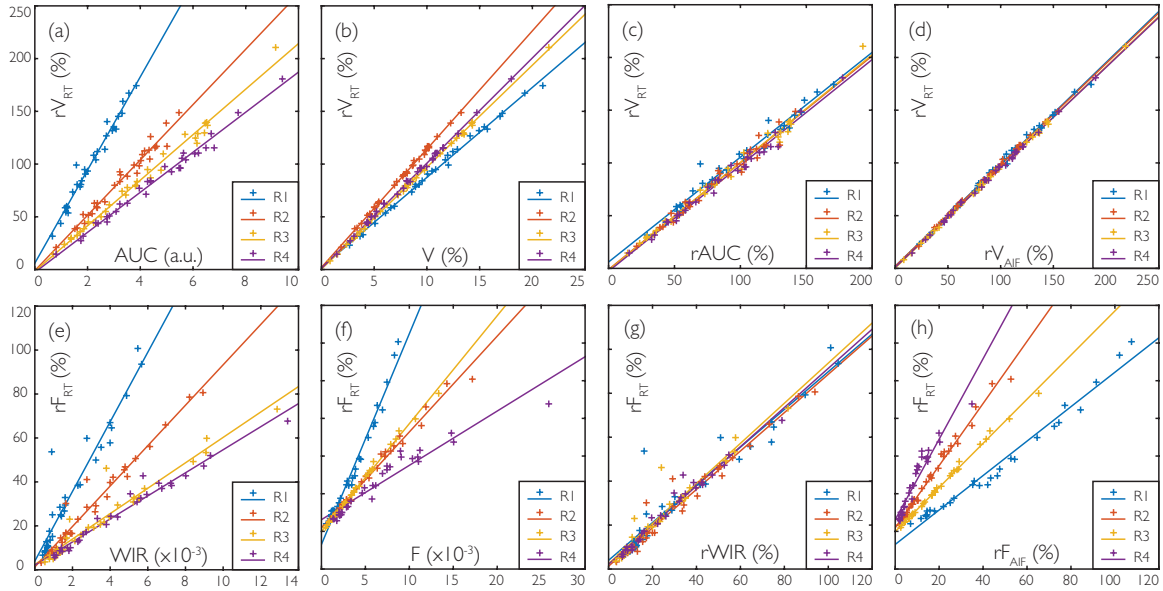

Figure 3-3: Comparison of the volume-based and flow-based parameters obtained for the four test-retest exams (R_1, R_2, R_3, and R_4) of the mouse m_1: linear regressions between (a) rV_{RT} and AUC, (b) rV_{RT} and V, (c) rV_{RT} and $rAUC$, (d) rV_{RT} and rV_{AIF}, (e) rF_{RT} and WIR, (f) rF_{RT} and F, (g) rF_{RT} and $rWIR$, (h) rF_{RT} and rF_{AIF}.

parameters ($rAUC$, rV_{AIF}, and rV_{RT}) have significantly lower CV than absolute volume parameters (AUC and V). No significant difference was found when comparing WIR, F, and $rWIR$, but the CV of these parameters are significantly higher than those of rF_{AIF} and rF_{RT}. Numerical values of these mean CV are given for each mouse in Appendix, in Table 3.5.

3.6 Discussion

Using a test-retest study with a controlled bolus injection, it was possible to assess the variability of DCE-US perfusion parameters. To reduce this variability, the interest of estimating relative parameters, which necessitates the definition of a reference tissue region, was practically demonstrated. Our study also shows the importance of choosing an appropriate method for the estimation of the parameters, because estimation methods have an impact on parameter variability. Thus the reference tissue approach (**rRTd**) can be recommended, since it is the most robust method when considering the volume-based and the flow-based parameters simultaneously.

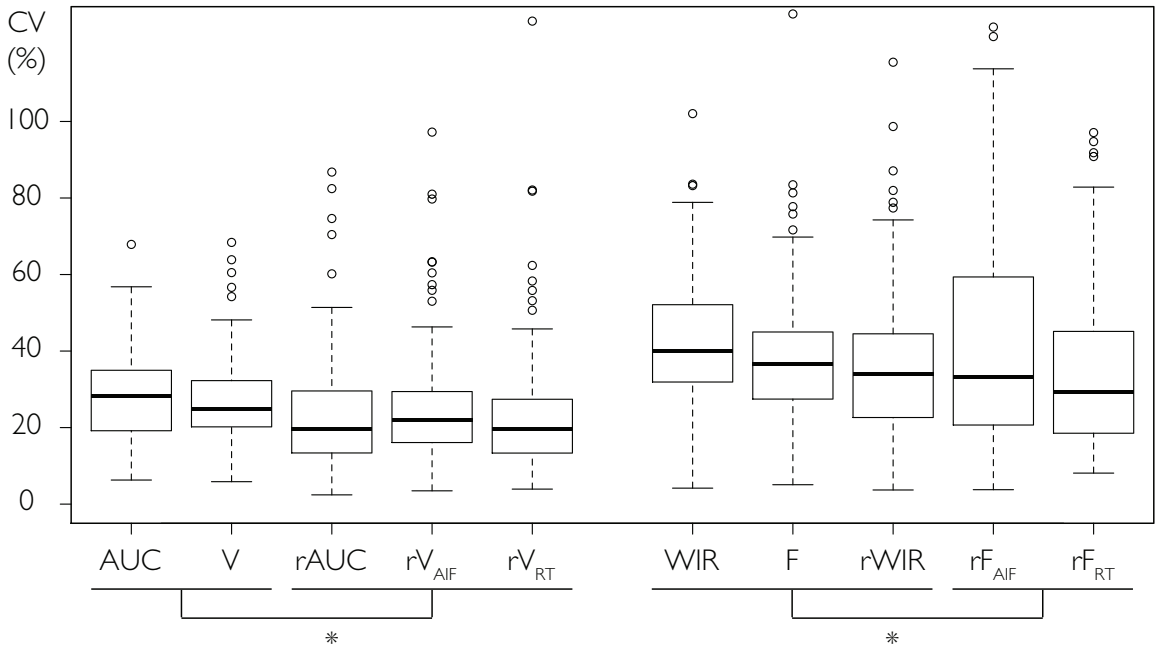

Figure 3-4: Boxplot showing the coefficients of variation of blood volume parameters (left) and blood flow parameters (right) estimated with the **aLN**, **rLN**, **aAIFd**, **rAIFd**, and **rRTd** models. For each box, the bold line represents the median value, the bottom and top lines the first and third quartiles. Dotted lines extend to the most extreme data points which are less than 1.5 times the interquartile range. Outlier points are displayed with empty circles. Two groups of parameters were built (horizontal lines below the parameter names) such that there were no significant intra-group differences while there were statistically significant inter-group differences (marked by *).

The recommendations of the EFSUMB for DCE-US quantification in oncology suggest to estimate parameters such as AUC and WIR from explicitly defined models, e.g. using the **aLN** model. To reduce the variability of the estimated parameters, Dizeux et al. proposed a controlled injection system [3]. However, the present study shows that the differences between two consecutive exams are still not negligible for a regional analysis. Since in PET and DCE-MRI, deconvolution approaches and compartmental models have proved their efficiency to make parameters more robust to inter-exam changes, we decided to test some of these approaches. The most commonly used methods require the estimation of an arterial input function. Deconvolution approaches were recently proposed to quantify tissue perfusion in DCE-US [5]. These approaches estimate the transfer function of the system (depending on a large number of parameters), and to avoid aberrant solutions, this estima-

tion needs to be regularized. Following this idea, the one-compartment model with time delay is a deconvolution depending on three parameters only. When the time delay is set to 0, (**aAIF** model), we have shown that the quality of fit is worse than the one obtained when using the explicit **aLN** model. When introducing a time delay parameter, an option that is unfortunately generally overlooked [11], a much more accurate fit of regional tumor kinetics was obtained. Indeed, the quality of fit using **aLN** (depending on four parameters) and this **aAIFd** model was equivalent in terms of $NRMSE$.

Our study shows the crucial role of the AIF estimation in the variability of the perfusion parameters (see Table 3.3). When focusing the field of view in the main plane of the tumor, it can be difficult to estimate the AIF robustly (see Figure 3-2). Indeed, AIF measurements in small vessels can be affected by partial volume effects, yielding underestimation of the signal intensity. Thus coefficients of variation deduced from the **aAIFd** model can be high. Note that some problems could also occur in larger vessels, including non-linearities between concentration and measured signal, and attenuation artifacts [13].

The use of relative parameters was suggested to overcome the difficulties of estimating the AIF for a compartmental model in DCE-MRI [25]. Clinical studies have reported the interest of estimating normalized perfusion parameters in DCE-US [6, 8, 12]. Using systematically three models (**rLN**, **rAIFd**, **rRTd**), our study reinforces the interest of estimating relative parameters. The choice of a reference tissue region is less critical than the segmentation of an artery. Indeed, a larger structure can be used, reducing segmentation errors and the impact of partial volume effect. Furthermore, as the contrast concentration is lower, the quantification errors due to non-linearity are reduced. Kidney regions were initially tested but finally excluded because of the overlap of cortical, proximal tubular and distal tubular compartments. Muscular regions that could be delineated on the four exams were finally chosen.

Recirculation is a major problem when dealing with modeling techniques adapted to first-pass studies. However, its quantitative impact is reduced in DCE-US when compared to other modalities since the destruction of microbubbles, in the lungs in particular, makes the number of microbubbles much smaller in the second pass (and following) than it is in the first pass. We deliberately did not try to model the recirculation, when we chose the **aLN**

model to fit tumor kinetics or when we first fit the AIF using the **aLN** model. In addition, using simulated data, we showed that the practical impact on parameters estimation when neglecting the recirculation was limited, especially for relative parameters, since the coefficients of variation between parameters estimated with and without simulating the recirculation effect were less than the ones estimated through the test-retest studies (this recirculation effect was about 5% on CV values with the **rRTd** approach).

The use of normalized parameters induced a significant reduction of coefficients of variation in our test-retest study. Furthermore, estimating relative volume and flow parameters using equation (3.5), which eliminates the need for an AIF, is more robust than using the AIF directly. It should also be noted that the small 3D displacements occurring between the four test-retest studies can partly explain the CV, due to the imperfect spatial alignment between sub-regions from one exam to the following one.

Figure 3-3 reveals strong correlations between the different parameters computed inside a same sub-region, and a large variation of these parameters according to the tumor sub-regions. Thus, whatever the model used, all the flow-based or volume-based parameters can reveal spatial tumor heterogeneity. However, when it comes to the comparison of longitudinal exams, it is crucial to have comparable parameter values. Thus, the estimation of relative parameters seem to be the most powerful solution, provided that the reference tissue characteristics are not modified between exams. Some interesting results have been recently shown [22] for a longitudinal study using a 3D DCE-US approach. Compared with the 2D approach, the 3D approach enables assessment of the whole tumor and should be preferred for tumor monitoring.

3.7 Conclusion

This study aimed at proposing valuable modeling of DCE-US studies to estimate reliable perfusion parameters in a murine model of tumor. First, it was shown that a one-compartment model based on an AIF, and completed by the estimation of a time-delay parameter, could fit kinetics as closely as the explicit log-normal model. Second, a comprehensive comparison of the parameters estimated by different approaches was proposed, showing high correla-

tions between the volume-based and flow-based parameters respectively estimated. Based on test-retest studies with controlled injections, a large variability (up to 40%) of regional perfusion parameters was established due to the inherent variations of experimental and physiological conditions for the log-normal modeling and to the difficulties in estimating a correct AIF in the image field of view for the compartmental approach. To reduce this variability, the use of relative values of these regional perfusion parameters was proposed, requiring in all cases the delineation of a reference tissue region. To estimate these relative parameters, the reference tissue model proved to be the most reliable computing approach. Thus we recommend the use of this model to estimate reliable relative perfusion parameters.

3.8 Acknowledgments

The authors are grateful to the anonymous reviewers for their valuable comments on the paper. This work was funded by the Fondation pour la Recherche Médicale through the Bio-ingénierie pour la Santé research grant DBS20131128436. Research was also supported by the Institut Universitaire d'Ingénierie en Santé, Sorbonne Université, Projet OCSCC 2014/2016. Experiments were performed on a platform of France Life Imaging partly funded by the grant ANR-11-INBS-0006 associated within the Plateforme Imagerie du Vivant. All the animals were house kept at Centre d'Ex-plorations Fonctionnelles of Centre de Recherche des Cordeliers, Agreement A75-06-12.

References

Bibliography

[1] Daniel Balvay, Frédérique Frouin, Guillaume Calmon, Bertrand Bessoud, Edmond Kahn, Nathalie Siauve, Olivier Clément, and Charles A Cuenod. New criteria for assessing fit quality in dynamic contrast-enhanced T1-weighted MRI for perfusion and permeability imaging. *Magn Reson Med*, 54(4):868–877, 2005. 55

[2] C F Dietrich, Michalakis Averkiou, J-M Correas, N Lassau, E Leen, and F Piscaglia. An EFSUMB introduction into Dynamic Contrast-Enhanced Ultrasound (DCE-US) for quantification of tumour perfusion. *Ultraschall Med*, 33(4):344–351, August 2012. 48, 52

[3] Alexandre Dizeux, Thomas Payen, Guillaume Barrois, Delphine Le Guillou-Buffello, and S Lori Bridal. Reproducibility of Contrast-Enhanced Ultrasound in mice with controlled injection. *Mol Imaging Biol*, 18(5):651–658, October 2016. 49, 50, 59

[4] Maxime Doury, Alexandre Dizeux, Alain De Cesare, Olivier Lucidarme, S Lori Bridal, and Frédérique Frouin. Comparison of the reproducibility of perfusion parameters obtained in CEUS studies with three modeling approaches. In *Proc IEEE Int Symp Biomed Imaging*, Prague, February 2016. 49

[5] Marianne Gauthier, Farid Tabarout, Ingrid Leguerney, Mélanie Polrot, Stéphanie Pitre, Pierre Peronneau, and Nathalie Lassau. Assessment of quantitative perfusion parameters by dynamic contrast-enhanced sonography using a deconvolution method: an in vitro and in vivo study. *J Ultrasound Med*, 31(4):595–608, April 2012. 49, 59

[6] Aymeric Guibal, Laurent Taillade, Sébastien Mulé, Eva Comperat, Yasmina Badachi, Jean Louis Golmard, Delphine Le Guillou-Buffello, Olivier Rixe, S Lori Bridal, and Olivier Lucidarme. Noninvasive contrast-enhanced US quantitative assessment of tumor microcirculation in a murine model: effect of discontinuing anti-VEGF therapy. *Radiology*, 254(2):420–429, February 2010. 60

[7] R N Gunn, S R Gunn, and V J Cunningham. Positron emission tomography compartmental models. *J Cereb Blood Flow Metab*, 21(6):635–652, 2001. 52

[8] C Hoeffel, S Mulé, L Huwart, Frédérique Frouin, J P Jais, O Helenon, and J-M Correas. Renal blood flow quantification in pigs using contrast-enhanced ultrasound: an ex vivo study. *Ultraschall Med*, 31(4):363–369, April 2010. 60

[9] T Hothorn, K Hornik, MA van de Wiel, and A Zeileis. Implementing a Class of Permutation Tests: The coin Package. *Journal of Statistical Software*, 28(8):1–23, 2008. 55

[10] Radovan Jirik, Karel Soucek, Martin Mezl, Michal Bartos, Eva Drazanova, Frantisek Drafi, Lucie Grossova, Jiří Kratochvíla, OndrÌĘej MacicÌĘek, Kim Nylund, Ales Hampl, Odd Helge Gilja, Torfinn Taxt, and Zenon Starcuk. Blind deconvolution in dynamic contrast-enhanced MRI and ultrasound. *Conf Proc IEEE Eng Med Biol Soc*, 2014:4276–4279, 2014. 49

[11] Kohsuke Kudo, Makoto Sasaki, Kuniaki Ogasawara, Satoshi Terae, Shigeru Ehara, and Hiroki Shirato. Difference in tracer delay–induced effect among deconvolution algorithms in CT perfusion analysis: quantitative evaluation with digital phantoms. *Radiology*, 251(1):241–249, April 2009. 60

[12] Thibaud Lefort, Frank Pilleul, Sébastien Mulé, S Lori Bridal, Frédérique Frouin, Catherine Lombard-Bohas, Thomas Walter, Olivier Lucidarme, and Aymeric Guibal. Correlation and agreement between contrast-enhanced ultrasonography and perfusion computed tomography for assessment of liver metastases from endocrine tumors: normalization enhances correlation. *Ultrasound Med Biol*, 38(6):953–961, June 2012. 60

[13] Sébastien Mulé, Alain de Cesare, Olivier Lucidarme, Frédérique Frouin, and Alain Herment. Regularized Estimation of Contrast Agent Attenuation for Improvement of Microbubble Imaging in Small Animal Studies. *Ultrasound Med Biol*, 34(6):938–948, 2008. 60

[14] J P B O'Connor, A Jackson, G J M Parker, and G C Jayson. DCE-MRI biomarkers in the clinical evaluation of antiangiogenic and vascular disrupting agents. *Br J Cancer*, 96(2):189–195, January 2007. 48

[15] Clifford S Patlak, Ronald G Blasberg, and Joseph D Fenstermacher. Graphical evaluation of blood-to-brain transfer constants from multiple-time uptake data. *J Cereb Blood Flow Metab*, 3(1):1–7, March 1983. 54

[16] Thomas Payen, Alain Coron, Michele Lamuraglia, Delphine Le Guillou-Buffello, Emmanuel Gaud, Marcel Arditi, Olivier Lucidarme, and S Lori Bridal. Echo-Power es-

timation from log-compressed video data in dynamic contrast-enhanced ultrasound imaging. *Ultrasound Med Biol*, 39(10):1826–1837, October 2013. 50

[17] Costas Strouthos, Marios Lampaskis, Vassilis Sboros, Alan McNeilly, and Michalakis Averkiou. Indicator dilution models for the quantification of microvascular blood flow with bolus administration of ultrasound contrast agents. *IEEE Trans Ultrason Ferroelectr Freq Control*, 57(6):1296–1310, June 2010. 48, 52

[18] M X Tang, H Mulvana, T Gauthier, A K P Lim, D O Cosgrove, R J Eckersley, and E Stride. Quantitative contrast-enhanced ultrasound imaging: a review of sources of variability. *Interface Focus*, 1(4):520–539, June 2011. 48

[19] Paul S Tofts, Gunnar Brix, David L Buckley, Jeffrey L Evelhoch, Elizabeth Henderson, Michael V Knopp, Henrik B Larsson, Ting-Yim Lee, Nina A Mayr, Geoffrey J Parker, Ruediger E Port, June Taylor, and Robert M Weisskoff. Estimating kinetic parameters from dynamic contrast-enhanced T(1)-weighted MRI of a diffusable tracer: standardized quantities and symbols. *J Magn Reson Imaging*, 10(3):223–232, 1999. 48

[20] A Tudorica, H Fang Li, F Hospod, E Delucia-Deranja, W Huang, CS Patlak, and GC Newman. Cerebral blood volume measurements by rapid contrast infusion and T2*-weighted echo planar MRI. *Magn Reson Med*, 47(6):1145–1157, June 2002. 52

[21] Stef van Buuren and Karin Groothuis-Oudshoorn. mice: Multivariate Imputation by Chained Equations in R. *J Stat Softw*, 45(1):1–67, December 2011. 55

[22] Huaijun Wang, Dimitre Hristov, Jiale Qin, Lu Tian, and Jürgen K Willmann. Three-dimensional dynamic Contrast-enhanced US imaging for early antiangiogenic treatment assessment in a mouse colon cancer model. *Radiology*, 277(2):424–434, November 2015. 61

[23] Suparna Bonthala Wedam, Jennifer A Low, Sherry X Yang, Catherine K Chow, Peter Choyke, David Danforth, Stephen M Hewitt, Arlene Berman, Seth M Steinberg, David J Liewehr, Jonathan Plehn, Arpi Doshi, Dave Thomasson, Nicole McCarthy, Hartmut Koeppen, Mark Sherman, JoAnne Zujewski, Kevin Camphausen, Helen

Chen, and Sandra M Swain. Antiangiogenic and antitumor effects of bevacizumab in patients with inflammatory and locally advanced breast cancer. *J Clin Oncol*, 24(5): 769–777, February 2006. 48

[24] K Wei, A R Jayaweera, S Firoozan, A Linka, D M Skyba, and S Kaul. Quantification of myocardial blood flow with ultrasound-induced destruction of microbubbles administered as a constant venous infusion. *Circulation*, 97(5):473–483, February 1998. 48

[25] Thomas E Yankeelov, Jeffrey J Luci, Martin Lepage, Rui Li, Laura Debusk, P Charles Lin, Ronald R Price, and John C Gore. Quantitative pharmacokinetic analysis of DCE-MRI data without an arterial input function: a reference region model. *Magn Reson Imaging*, 23(4):519–529, May 2005. 54, 60

Appendix

This appendix gives the numerical results that were obtained for each mouse (m_1, m_2, m_3, and m_4), including mean values and standard deviations of regional parameters (Table 3.4) and coefficients of variation of these parameters (Table 3.5).

	Absolute parameters		Relative parameters		
	AUC (a.u.)	V (%)	$rAUC$ (%)	rV_{AIF} (%)	rV_{RT} (%)
m_1	3.47 ± 1.82	8.61 ± 4.31	87.2 ± 37.9	87.6 ± 41.5	85.9 ± 41.2
m_2	5.97 ± 2.08	17.6 ± 6.60	11.2 ± 3.19	18.1 ± 6.25	13.2 ± 3.51
m_3	6.74 ± 3.51	12.9 ± 6.40	144 ± 81.3	131 ± 73.0	132 ± 75.2
m_4	7.90 ± 4.23	21.2 ± 11.6	57.9 ± 30.6	62.3 ± 33.1	59.4 ± 31.6
	WIR (a.u. s^{-1})	F (s^{-1})	$rWIR$ (%)	rF_{AIF}(%)	rF_{RT} (%)
m_1	3.30 ± 2.66	4.94 ± 4.07	29.7 ± 23.4	21.9 ± 21.9	27.0 ± 20.3
m_2	4.70 ± 3.03	6.49 ± 3.45	17.7 ± 10.2	17.2 ± 8.34	16.1 ± 11.0
m_3	4.88 ± 4.19	3.64 ± 2.90	32.9 ± 28.6	36.4 ± 27.7	25.1 ± 21.0
m_4	6.63 ± 5.30	5.21 ± 3.59	23.7 ± 19.0	26.4 ± 18.2	18.0 ± 13.6
Delay	Δ (s)	d (s)	D_{LN}^{T-R} (s)	D_{AIF}^{T-R} (s)	D_{RT}^{T-R} (s)
m_1	5.5 ± 3.4	3.2 ± 4.1	−1.9 ± 3.4	2.7 ± 4.2	3.9 ± 4.7
m_2	2.8 ± 2.5	5.7 ± 4.7	0.7 ± 2.4	4.2 ± 4.5	5.3 ± 4.0
m_3	3.2 ± 2.8	7.4 ± 5.6	0.4 ± 3.1	3.6 ± 5.5	4.4 ± 5.8
m_4	4.4 ± 2.4	7.0 ± 4.6	−0.8 ± 2.3	5.9 ± 4.5	5.6 ± 4.7

Table 3.4: Mean ± standard deviation of the volume, flow and delay parameters estimated in the different sub-regions of the tumor, for the four test-retest exams, after multiple imputation of missing values due to poor fit quality. Values of WIR and F are multiplied by 1000.

	Absolute parameters		Relative parameters		
	CV_{AUC}	CV_V	CV_{rAUC}	$CV_{rV_{AIF}}$	$CV_{rV_{RT}}$
m_1	34.7 ± 10.6	30.2 ± 17.1	22.4 ± 14.4	24.6 ± 17.5	24.7 ± 17.3
m_2	26.2 ± 6.83	26.7 ± 9.85	15.0 ± 6.51	21.8 ± 9.99	15.3 ± 7.01
m_3	31.0 ± 12.3	26.6 ± 10.9	37.2 ± 16.8	35.2 ± 17.8	35.2 ± 18.7
m_4	20.7 ± 10.6	23.3 ± 9.93	18.8 ± 8.68	19.0 ± 7.61	17.8 ± 8.17
	CV_{WIR}	CV_F	CV_{rWIR}	$CV_{rF_{AIF}}$	$CV_{rF_{RT}}$
m_1	42.4 ± 12.4	35.4 ± 12.5	33.4 ± 14.9	75.5 ± 19.9	29.6 ± 13.2
m_2	44.4 ± 11.0	34.4 ± 7.23	27.4 ± 10.9	23.4 ± 9.94	33.1 ± 18.7
m_3	45.3 ± 18.5	46.9 ± 17.7	50.9 ± 17.7	36.8 ± 16.6	38.3 ± 21.3
m_4	34.9 ± 18.9	33.3 ± 17.3	38.3 ± 21.2	27.1 ± 13.7	29.4 ± 15.8

Table 3.5: Mean ± standard deviation of the coefficients of variation (CV), expressed in percentage, of volume and flow parameters estimated for each sub-region after multiple imputation of missing values due to poor fit quality. CV were not computed for time delays, since their values can be either positive or negative.

Chapter 4

Regularized Linear Resolution of a One-Compartment Model to Improve the Reproducibility of Perfusion Parameters in CEUS

4.1 Abstract

Contrast-enhanced ultrasound (CEUS) has been proposed to monitor tumor therapy, in complement to size measurements. Estimating reliable perfusion parameters from CEUS studies is essential in order to propose adapted therapy options according to the parameter values. The variability of these parameters was assessed in an ideal case of consecutive test-retest CEUS studies, in a mouse tumor model. The impact of mathematical modeling on parameter variability was investigated on these data. Four models were compared in 32 tumor sub-regions : the log-normal model (LN), the relative LN model (rLN) where parameters of LN are normalized by the parameters estimated inside a reference tissue (RT) region, a linear resolution of a one-compartment model based on the RT (rLin), a modified version of rLin implementing regularization (rLinReg) to ensure coherent results between the different sub-regions of the tumor. Results show that LN model had highest coefficients

of variation. The positive impact of normalization using RT (rLN) was established, showing reduced coefficients of variation. The rLin approach showed large variations especially for flow parameters. Its regularization version, rLinReg, greatly improved parameter reproducibility while providing coherent results between the sub-regions. In conclusion,the rLinReg approach provided the smallest coefficients of variations and should be preferred for estimating perfusion parameters in CEUS.

4.2 Introduction

Reliable quantification of tumor perfusion is a challenging, yet necessary, milestone to reach in order to efficiently monitor tumor growth and treatment efficiency. Contrast-enhanced ultrasound (CEUS) is a non-invasive tool allowing real-time quantitative vascular imaging: for every sampling time and every pixel in the image, the linearized signal intensity is proportional to the concentration of contrast agent for low concentrations.

Recommendations for the quantification of CEUS studies rely on explicit modeling of time-intensity curves (TICs), e.g. using a log-normal model [3]. Then, semi-quantitative parameters are usually derived directly from the modeled TIC, e.g. area under the curve (AUC) and wash-in rate (WIR). These parameters are directly affected by inter-exam changes occurring either in physiology, e.g. heart rate, blood pressure, or in experimental conditions, e.g. injected quantity, or injection speed [7]. Controlled injections and compartmental modeling have been proposed to reduce this variability [4]. To overcome the issues related to the estimation of a correct arterial input function, the use of a reference tissue (RT) region (e.g. [2]) has been successfully tested [4]. In the present study, a linear formulation of the one-compartment model is presented and evaluated. This formulation allows the evaluation of an otherwise unidentifiable parameter, characterizing the RT region, which value had to be set arbitrarily to 0.15. To prove the interest of this new approach, the coefficients of variation of perfusion parameters estimated at a regional scale were compared using four different approaches: 1) the log-normal model (**LN**), 2) the relative LN model (**rLN**), where parameters are normalized by the (**LN**) parameters estimated inside the RT region, 3) a linear resolution of the one-compartment model based on the RT region (**rLin**), 4) a modified

version of **rLin** implementing regularization (**rLinReg**) to ensure a coherent estimation of the ratio between blood flow and blood volume in the RT region when taking into account the different sub-regions in the tumor.

4.3 Materials

4.3.1 Animals

All experiments were conducted in accordance with the institutional guidelines and the recommendations for the care and use of laboratory animals. They were based on a murine model of Lewis Lung Carcinoma (3LL). Tumor fragments (20-40 mm^3) were implanted 20 days prior to the CEUS acquisitions in the right flank of Balb/C mice. Anesthesia was maintained during the whole acquisition through a face mask delivering 2% isoflurane in air delivered at a 1 L/min rate.

4.3.2 Image acquisition

Tumors were imaged in their largest cross-section plane, mice motion was limited using surgical tape securing animal position during and between acquisitions. A controlled injection system was used to inject, at a rate of 4.5 mL/min, a 50 µL bolus of SonoVue (Bracco Suisse SA, Geneva, Switzerland) diluted to 20%. Meanwhile, dynamic contrast-enhanced US sequences were acquired using a 15L8W transducer coupled to a Sequoia 512 US system (Acuson, Siemens, Mountain View, CA, USA) in dual-mode, i.e. anatomical B-Mode along with Contrast Pulse Sequencing (CPS) images. Mechanical index was set to 0.1, dynamic range to 80 dB, and time gain compensation was applied. The frame rate was set to 3 Hz during the first 30 seconds (including the wash-in phase and the beginning of the wash-out phase), and 1 Hz for the remaining time.

For the four mice in the study, four consecutive (test-retest) data-sets were acquired without any modification in the setup. Fifteen minute breaks were observed between acquisitions to ensure the disruption of previously injected micro-bubbles.

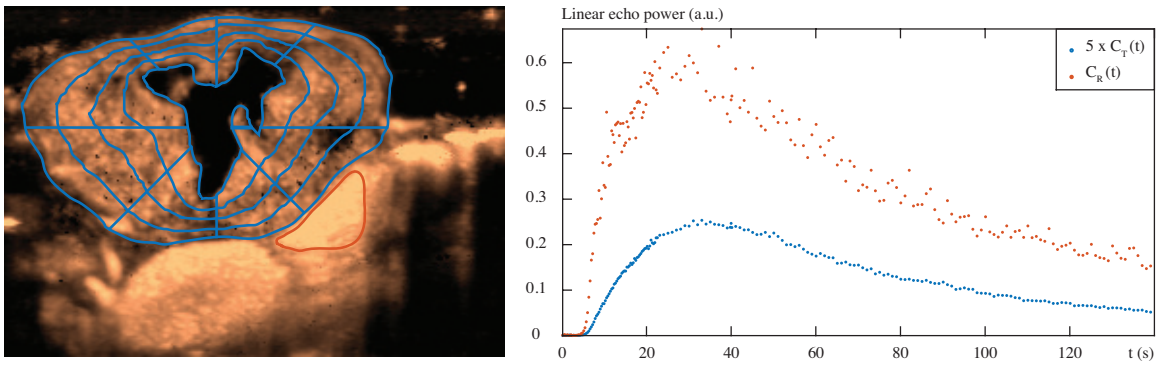

Figure 4-1: Illustration of the data pre-processing steps. Left: The contours of the perfused tumor area have been overlaid on a contrast-enhanced image (in blue color). This area was automatically divided into 4 radial layers and 8 angular sectors as shown by the spiderweb patterns. A RT region (in orange color) was also delineated. Right: Mean TICs associated with the perfused area of the tumor, and the RT.

4.4 Methods

4.4.1 Data pre-processing

Linear echo-power TICs were calibrated from log-compressed video data using a laboratory-made software. Both probe and animal motion were assumed negligible for the selected sequences.

Tumors (hereafter labeled with subscript T) were segmented on the B-Mode images and the non-perfused areas were removed for data analysis. In order to preserve the signal-to-noise-ratio (SNR) of the TICs while revealing the spatial heterogeneity of the tumor, a regional analysis of the tumor area was performed. The perfused tumor region was divided into $N_T = 32$ sub-regions according to 4 radial layers and 8 angular sectors (Figure 4-1). Then mean regional TICs $C_T^i(t)$, for $i = 1, ...N_T$ were computed. As three of the four quantification methods require the selection of a RT region, for each mouse, this RT region (hereafter labeled with subscript R) was chosen to be easily identifiable on the different test-retest studies. A muscular region close to the kidney was generally selected, the renal cortex being excluded from the RT region due to the complexity of perfusion patterns observed inside this structure.

Finally for each sub-region, a time delay parameter, D_i, representing the time of arrival

of the contrast agent in the considered region, was estimated as follows:

$$D_i = \max_t \frac{\mathrm{d}^2}{\mathrm{d}t^2}(C_T^i * W * W), \tag{4.1}$$

where W is an average filter with a fixed width empirically set to 2.0 seconds. Using this specific time delay, all regional TICs were registered in time for subsequent analysis.

4.4.2 Definition of the four models

Log-Normal model (LN)

This method based on the log-normal distribution was recommended by the EFSUMB for quantification of tumor perfusion in clinical studies [3]. The TIC inside the i^{th} region of the tumor, $C_T^i(t)$, is fitted according to equation (4.2):

$$\begin{aligned} C_T^i(t) &= \frac{A_T^i}{\sqrt{2\pi}\sigma_T^i t} \exp\left(-\frac{\left[\ln(t)-\mu_T^i\right]^2}{2{\sigma_T^i}^2}\right) \text{ if } t \geq 0, \\ &= 0 \text{ otherwise.} \end{aligned} \tag{4.2}$$

Regional parameters A_T^i, μ_T^i, and σ_T^i were estimated for each sub-region. Semi-quantitative parameters are then derived from the model, including AUC^i and WIR^i. These parameters depend, in a non-linear way, on the parameters of the **LN** model, A^i, μ^i, and σ^i. Relations have been established, both analytically and experimentally, between parameters derived from the **LN** model and physiological parameters, showing AUC^i is related to blood volume, and WIR^i to blood flow [4].

Normalized log-normal model (rLN)

Regional relative parameters: $rAUC^i$ and $rWIR^i$ were derived from the parameters estimated with the (**LN**) model in the tumor sub-regions (AUC_T^i, WIR_T^i) and those estimated in the RT region (AUC_R, WIR_R). They were defined as follows:

$$\begin{cases} rAUC^i &= AUC_T^i / AUC_R, \\ rWIR^i &= WIR_T^i / WIR_R. \end{cases} \tag{4.3}$$

Simple one-compartment model (rLin)

The resolution of the one-compartment model follows the graphical analysis technique introduced by Patlak et al. for the quantification of irreversible tracers in PET. The method, based on compartmental modeling, estimates blood-related physiological parameters by means of linear regression, assuming the arterial input function (AIF) is known [6]. This linear approach is generalized to reversible tracers [5]. These approaches have also been adapted to relax the need for blood sampling or AIF measurement and the kinetics inside a RT region was then used (see for instance [2]). This resolution was adapted to CEUS data, considering the ultrasound contrast agent is strictly intra-vascular. Considering a one-compartment model to describe flow exchanges inside the tissue, the following equations can be written for each sub-region, $i = 1, \ldots, N_T$:

$$\frac{\mathrm{d}C_T^i(t)}{\mathrm{d}t} = F_T^i.C_A(t) - \frac{F_T^i}{V_T^i}C_T^i(t). \tag{4.4}$$

In (4.4) $C_A(t)$ represents the arterial input function feeding the tissue, while V_T^i stands for the fractional blood volume, and F_T^i for the blood flow in the sub-region i.

Considering jointly the TIC inside the RT region and the TICs in the tumor, and assuming a common feeding input for the RT region and the tumor, we have the following set of equations:

$$\begin{cases} \frac{\mathrm{d}C_R(t)}{\mathrm{d}t} &= F_R.C_A(t) - \frac{F_R}{V_R}C_R(t), \\ \frac{\mathrm{d}C_T^i(t)}{\mathrm{d}t} &= F_T^i.C_A(t) - \frac{F_T^i}{V_T^i}C_T^i(t), \forall i. \end{cases} \tag{4.5}$$

Rearranging the first equation, $C_A(t)$ can be isolated and expressed as a function of $C_R(t)$, and then replaced by its new expression in the N_T following equations, yielding the next system:

$$\begin{cases} C_A(t) &= \frac{1}{F_R}\frac{\mathrm{d}C_R(t)}{\mathrm{d}t} + \frac{1}{V_R}C_R(t), \\ \frac{\mathrm{d}C_T^i(t)}{\mathrm{d}t} &= \frac{F_T^i}{F_R}\frac{\mathrm{d}C_R(t)}{\mathrm{d}t} + \frac{F_T^i}{V_R}C_R(t) - \frac{F_T^i}{V_T^i}C_T^i(t). \end{cases} \tag{4.6}$$

After integration over time (from 0 to t), and definition of the parameters $rF^i = F_T^i/F_R$, $rV^i = V_T^i/V_R$, and $k_T^i = F_T^i/V_T^i$, the last equations of the system become:

$$C_T^i(t) = rF^i C_R(t) + rV^i k_T^i \int_0^t C_R(\tau)\,\mathrm{d}\tau - k_T^i \int_0^t C_T^i(\tau)\,\mathrm{d}\tau. \tag{4.7}$$

For each sub-region i, a sub-system of N linear equations (5.7) is computed, obtained for N successive values of t. N is the total number of dynamic frames. Solving this sub-system of N linear equations, the parameters rF^i, rV^i, and k_T^i can thus be estimated in the least-squares sense. Using this approach, the N_T linear equations corresponding to the different sub-regions are thus solved independently.

Regularization of the one-compartment model (rLinReg)

Using the previously described **rLin** model, N_T different values of $k_R = F_R/V_R$ can be derived, using the estimation of rF^i, rV^i, and k_T^i and the relation between the four parameters:

$$k_R = \frac{F_R}{F_T^i}\frac{F_T^i}{V_T^i}\frac{V_T^i}{V_R} = \frac{rV^i.k_T^i}{rF^i} \quad \text{for } i = 1,\ldots,N_T. \tag{4.8}$$

As the k_R values do not depend on sub-region i, the simple estimation proposed by **rLin** can introduce some inconsistencies k_R and possible biases in some rF^i, rV^i, and k_T^i values. To solve this issue, and consider one single value for k_R (whatever the number of sub-regions in the tumor), the regularized approach solves the system of equations (Eq. 5.7), under the following constraints:

$$\frac{rV^i.k_T^i}{rF^i} = K, \quad \forall i = 1,\ldots,N_T, \tag{4.9}$$

where K is a constant (equal to k_R). The system is solved globally for the N_T sub-regions. Briefly, the value of k_R is successively modified, thus providing a unique least-squares solution for the $3N_T$ parameters (rF^i, rV^i, and k_T^i), until the optimization of the fit for the whole set of N_T sub-regions.

4.4.3 Data analysis

For each model, a vector (Θ) of M perfusion parameters (θ_m) was estimated in each tumor sub-region ($i = 1,\ldots,32$) of each mouse ($j = 1,\ldots,4$) for each repeated acquisition ($k = 1,\ldots,4$), providing 512 results of curve fitting, Θ_k^{ij}, per model. The fit quality was assessed quantitatively, using the fraction of modeled information, FMI, according to [1].

The reproducibility of the perfusion parameters was then deduced for each sub-region of

each mouse by computing coefficients of variation $CV(\theta_m)^{ij}$ defined for the four repeated studies, as the ratio between the standard deviation and the mean value μ_m^{ij} of the parameter $(\theta_m)_k^{ij}$:

$$CV(\theta_m)^{ij} = \frac{\sqrt{\frac{1}{4}\sum_{k=1}^{4}((\theta_m)_k^{ij} - \mu_m^{ij})^2}}{\mu_m^{ij}}. \tag{4.10}$$

Parameters corresponding to poor quality fits ($FMI > 90\%$) were replaced using multivariate imputation by chained equations with the R module {mice} [8]. This strategy was defined to compute the CV using four values systematically.

Statistical tests were finally applied to compare the CV of the parameters estimated using the four models. Significant differences in the CV distributions were assessed using the Friedman test and the associated post-hoc analysis for multiple comparisons. Distribution means were considered as significantly different when p-values were less than 0.05.

4.5 Results

Model	**LN**	**rLN**	**rLin**	**rLinReg**
FMI	99.3%	99.3%	98.8%	98.1%
N_{rem}	28	28	1	39

Table 4.1: Median values of FMI obtained for the four models and number of sub-regions N_{rem}, out of 512, for which $FMI < 90\%$.

Table 4.1 shows the median values of the FMI obtained for the four models and the number of regions excluded from further statistical analysis because of bad fit quality.

Figure 4-2 displays a boxplot of the 128 coefficients of variation of blood volume parameters and blood flow parameters obtained for the four models **LN**, **rLN**, **rLin**, and **rLinReg**.

The p-values obtained after the post-hoc analysis of the Friedman test are shown in Table 4.2, significant differences in parameter distributions are emphasized in bold.

In terms of blood volume parameters, the **LN** model is the most variable with a median value of the coefficient of variation (CV) equal to 28.5%. Using the **rLin** model, the median CV tends to be lower (22.2%), however the difference is not statistically significant. Models

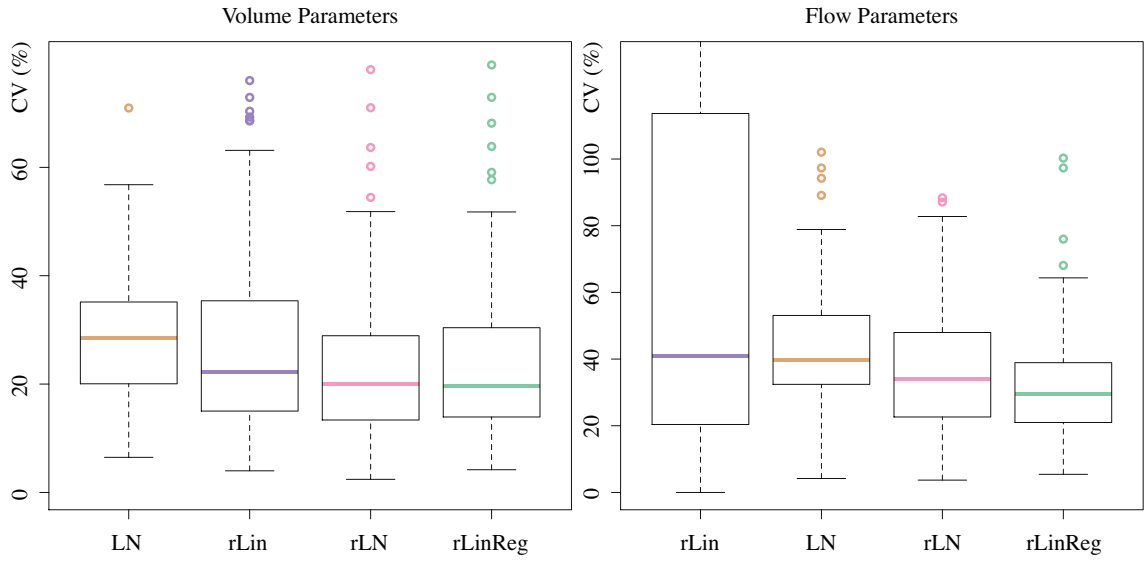

Figure 4-2: Boxplot showing the CV of blood volume (left) and blood flow (right) estimated with the **LN**, **rLN**, **rLin**, and **rLinReg** models.

	Volume parameters			Flow parameters		
	rLinReg	**rLin**	**rLN**	**rLinReg**	**rLin**	**rLN**
LN	**0.001**	0.1	**0.003**	$\mathbf{7 \times 10^{-6}}$	0.96	0.74
rLN	0.995	0.73		$\mathbf{5 \times 10^{-4}}$	0.49	
rLin	0.52			$\mathbf{8 \times 10^{-7}}$		

Table 4.2: p-values obtained in the post-hoc analysis of the Friedman test. Significant results ($p < 0.05$) in bold.

rLN and **rLinReg** yield significantly more reproducible blood volume parameters than **LN**, with median CV values of 20.0% and 19.7%, respectively. For the blood flow parameters, models **rLin** and **LN** appear to the most variable parameters with medians of CV equal to 40.8% and 39.6%, respectively. The **rLN** model tends to yield lower CV, with a median value of 34.1%. Finally the mean CV of blood flow using the **rLinReg** model is equal to 29.4%. It is significantly lower than the CV of blood flow obtained with the three other models.

4.6 Discussion

The number of sub-regions was chosen to reveal some spatial heterogeneity in the vascular network of the tumor, while ensuring regions were large enough to guarantee reasonable signal to noise ratios in regional TICs. Increasing the number of regions would reveal spatial heterogeneity more finely, at the expense of the accuracy of the estimates.

Both physiological and experimental variations get in the way of accurate quantification and exam comparison, affecting blood circulation, as well as measurements accuracy [7]. The semi-quantitative parameters of the **LN** model, recommended for tumor quantification, were found highly sensitive to inter-exam changes in our study and resulted in the least reproducible parameters.

When compared to the **LN** model, the normalized version, the **rLN** model reduces the variability of parameters. If the reduction of variability for blood flow parameters was not statistically significant, it was significant for blood volume parameters. Thus normalization using a RT region has a real potential to improve exam comparison.

Similarly to the **rLN** approach, the **rLin** model uses the RT region, but in addition, it assumes a one-compartment model to describe contrast exchanges between large vessels and micro-vascular areas in tissue. The first resolution method, which was tested in the present study and proposes to estimate three unknown parameters per sub-region, yields highly variable parameters, especially in terms of blood flow. However, the median CV of blood volume was reduced when compared to AUC CV, estimated with the **LN** model. This method was implemented in a naive way, resulting in inconsistent values of parameter k_R in the different tumor sub-regions.

The **rLinReg** model was built to overcome these inconsistencies, ensuring a single value of k_R. Enforcing a common value of k_R in sub-regions comes down to impose a fixed ratio between the first and second terms of Eq. 5.7. The number of degrees of freedom was thus reduced. The combined use of normalization through a RT region and regularization respects the compartmental modeling paradigm while yielding the most reproducible parameters in our study.

4.7 Conclusion

Using the **LN** model, derived parameters have high coefficients of variation. The positive impact of normalization using a reference tissue region on parameter reproducibility was established. The **rLinReg** approach takes into account the different sub-regions involved in the quantification, yielding a single value of parameter k_R common to all tumor sub-regions. In addition, this spatial regularization significantly reduces coefficients of variations of the blood flow parameter and should therefore be preferred to estimate spatially-distributed perfusion parameters.

Bibliography

[1] Daniel Balvay, Frédérique Frouin, Guillaume Calmon, Bertrand Bessoud, Edmond Kahn, Nathalie Siauve, Olivier Clément, and Charles A Cuenod. New criteria for assessing fit quality in dynamic contrast-enhancedT1-weighted MRI for perfusion and permeability imaging. *Magnetic Resonance in Medicine*, 54(4):868–877, 2005. 75

[2] Julio Cárdenas-Rodríguez, Christine M Howison, and Mark D Pagel. A linear algorithm of the reference region model for DCE-MRI is robust and relaxes requirements for temporal resolution. *Magnetic resonance imaging*, 31(4):497–507, May 2013. 70, 74

[3] C F Dietrich, Michalakis Averkiou, J-M Correas, N Lassau, E Leen, and F Piscaglia. An EFSUMB introduction into Dynamic Contrast-Enhanced Ultrasound (DCE-US) for quantification of tumour perfusion. In *Ultraschall in der Medizin (Stuttgart, Germany : 1980)*, pages 344–351. Innere Medizin 2, Caritas-Krankenhaus, Bad Mergentheim. Christoph.Dietrich@ckbm.de, © Georg Thieme Verlag KG, August 2012. 70, 73

[4] Maxime Doury, Alexandre Dizeux, Alain De Cesare, Olivier Lucidarme, Claire Pellot-Barakat, S Lori Bridal, and Frédérique Frouin. Quantification of tumor perfusion using dynamic contrast-enhanced ultrasound: impact of mathematical modeling. *Physics in medicine and biology*, 62(3):1113–1125, February 2017. 70, 73

[5] J Logan, J S Fowler, N D Volkow, A P Wolf, S L Dewey, D J Schlyer, R R MacGregor,

R Hitzemann, B Bendriem, and S J Gatley. Graphical analysis of reversible radioligand binding from time-activity measurements applied to [N-11C-methyl]-(-)-cocaine PET studies in human subjects. *Journal of Cerebral Blood Flow & Metabolism*, 10(5):740–747, September 1990. 74

[6] Clifford S Patlak, Ronald G Blasberg, and Joseph D Fenstermacher. Graphical Evaluation of Blood-to-Brain Transfer Constants from Multiple-Time Uptake Data. *Journal of Cerebral Blood Flow & Metabolism*, 3(1):1–7, March 1983. 74

[7] M X Tang, H Mulvana, T Gauthier, A K P Lim, D O Cosgrove, R J Eckersley, and E Stride. Quantitative contrast-enhanced ultrasound imaging: a review of sources of variability. *Interface Focus*, 1(4):520–539, August 2011. 70, 78

[8] Stef van Buuren and Karin Groothuis-Oudshoorn. mice: Multivariate Imputation by Chained Equations in R. *Journal of Statistical Software*, 45(1):1–67, December 2011. 76

Chapter 5

Impact of Recirculation in Dynamic Contrast-Enhanced Ultrasound: a Simulation Study

5.1 Abstract

Objectives The impact of recirculation on the quantification of perfusion is often neglected. It can however introduce a bias or some variability in the estimation of perfusion parameters and thus hamper comparison between exams. *Methods* Time-intensity curves (TICs) were simulated using a one-compartment model fed by an arterial input function (AIF). A simple model was developed to simulate recirculation in the AIF. Using AIF with and without recirculation, and sets of regional perfusion parameters, TICs corresponding to different tissue regions were simulated by convolution of the AIFs with the transfer function associated to each region. 150 simulations for each of the 10 noise levels were then computed. For each simulated study, six quantification methods based on either Log-Normal modeling or relative compartmental modeling were tested. Variations of the conventional Log-Normal model were also investigated, including using parameters estimated in a reference tissue for normalization purposes, and fitting only the first phase of the TIC to avoid recirculation. *Results* The impact of recirculation varies according to the quantification method. Restricting

parameter estimation to the first samples of the TICs, before recirculation occurs, appears to be the worst strategy. Errors are largely minimized when using a reference tissue to establish relative parameters. The most robust approach is the compartmental modeling based on a reference tissue and applied to multiple regions with a regularization constraint. *Conclusion* This simulation study demonstrates the influence of recirculation on the estimation of perfusion parameters. To reduce the impact of this unavoidable effect, the quantification method based on compartmental modeling and using a reference tissue appear to be the most reliable strategy.

5.2 Introduction

With the advent of contrast agents, perfusion imaging has been developed for different medical imaging modalities, including PET, CT, MRI, and more recently ultrasound. Perfusion parameters including regional tissue blood volume and tissue blood flow are functional indices which can help in the diagnosis of some vascular abnormalities, such as ischemia. Vascular modification in tumors is also a key application of perfusion imaging and can be used in order to assess tumor diagnosis or tumor monitoring [4].

A widely used approach to estimate perfusion parameters relies on bolus injections of contrast agent and dynamic recording of frames. However the quantification of signal and the estimation of perfusion parameters through mathematical modeling remains a hard task and has generated a lot of research work [12]. An accurate and robust estimation of perfusion parameters is of course crucial to compare perfusion imaging exams meaningfully. This is primordial in order to allow inter-subject exams or to perform monitoring. Among the different mathematical models that have been proposed in contrast-enhanced ultrasound (CEUS) studies, little attention has been devoted to compartmental modeling, despite its wide use in PET or MRI studies. Indeed, explicit modeling using for instance a Log-Normal function is often recommended to analyze dynamic data [4, 11]. Of course different reasons can explain this restricted use of the comparmental approach; among them the difficulty in estimating a correct arterial input function in dynamic ultrasound images can be cited. To get rid of this difficulty which occurs also while using other imaging techniques, some

authors in PET imaging and more recently in MRI have proposed to use a reference tissue in order to define relative perfusion parameters [3, 13], defined as the ratio between the perfusion parameters in the tissue of interest and the perfusion parameters defined in the reference tissue. Our group has recently shown the practical interest of this approach in a test-retest protocol applied to a murine tumor model [5, 6].

As no absolute gold-standard exist for preclinical or clinical studies, simulations can be used to assess the performance of different models and compare them. Of course, as it is quite complex to reproduce in silico the complexity of in vivo, the extrapolation of simulations to real cases should be done very carefully. However they can be used to focus on one specific trait and to quantify its impact. In the present study, the studied trait was recirculation, since this process is often overlooked when quantifying CEUS exams. This is especially true in small animals, where recirculation occurs quickly and can overlap with the first pass of the bolus of micro-bubbles in tissues, affecting the time-intensity curves (TICs) used for quantification.

For the present study, a one-compartmental model was assumed to be representative of the underlying physiology that is observable at a regional scale. Different values of perfusion parameters (tissue blood flow, tissue blood volume and time-delays) were simulated in order to better apprehend the spatial heterogeneity that can be observed inside a tumor. The values of these parameters were derived from results obtained in a preclinical study in order to be coherent with practical observations. In addition to recirculation, the impact of signal to noise ratio was studied. For the modelling apporach, two versions of the Log-Normal model (absolute and relative), and two versions of the relative one-compartment model (one based on a single region, one taking advantage from the existence of multiple regions) were considered. In addition, in order to limit the impact of recirculation while estimating perfusion parameters with the Log-Normal model, a simple and popular strategy was tested which consists in using the first samples of TICs, i.e. samples acquired before recirculation occurs [9]. These six perfusion quantification methods were fitted to simulated TICs to study the precision and the accuracy of the estimated perfusion parameters.

5.3 Theory

5.3.1 One-compartment vascular model

Consider N vascularized tissue regions T_i, $i = 1, .., N$ in a spatial domain, each region being an homogeneous compartment fed by the same arterial input function (AIF), C_A. This mono-compartmental hypothesis is realistic since the distribution of microbubbles is restricted to the vascular space [7]. Each tissue TIC, C_{T_i}, is characterized by a tissue blood volume V_i, and a tissue blood flow F_i. Since introducing a time-delay parameter in this model was shown to improve the quality of fit in tumor tissues [6], a parameter D_i reflecting the transit time of the contrast agent from the feeding artery to the tissue was also considered. The mathematical relationship between the tissue TIC and the TIC in its feeding artery is given by equation 5.1:

$$C_{T_i} = C_A * h_{F_i,V_i,D_i} \tag{5.1}$$

where $h_{F_i,V_i,D_i}(t) = F_i \cdot \mathrm{e}^{-\frac{F_i}{V_i}(t-D_i)} \forall\, t \leq D_i, 0$ else, represents the transfer function of the i^{th} tissue region.

5.3.2 Simplified recirculation model

After injection in a vein, the bolus of microbubbles travels through the lungs and heart chambers before being distributed in the whole body through the arterial system. After this first pass in the tissues, microbubbles return to the venous system for another circulation loop. During each loop, the bolus is attenuated by the natural disruption of microbubbles, and their filtration through the lungs and the liver. Additionally, the bolus length spreads in time because of the inhomogeneous path length of the individual microbubbles [2].

An AIF with recirculation, C_{Aw}, can therefore be approximated by a sum of consecutive passes of the bolus in the region of interest (equation 5.2):

$$C_{Aw}(t) = C_{A1}(t) + \sum_{r=1}^{N_R} R_r(t), \tag{5.2}$$

where $C_{A1}(t)$ is the TIC of the first pass of the bolus, $R_r(t)$ is the TIC of the r$^{\text{th}}$ recirculation,

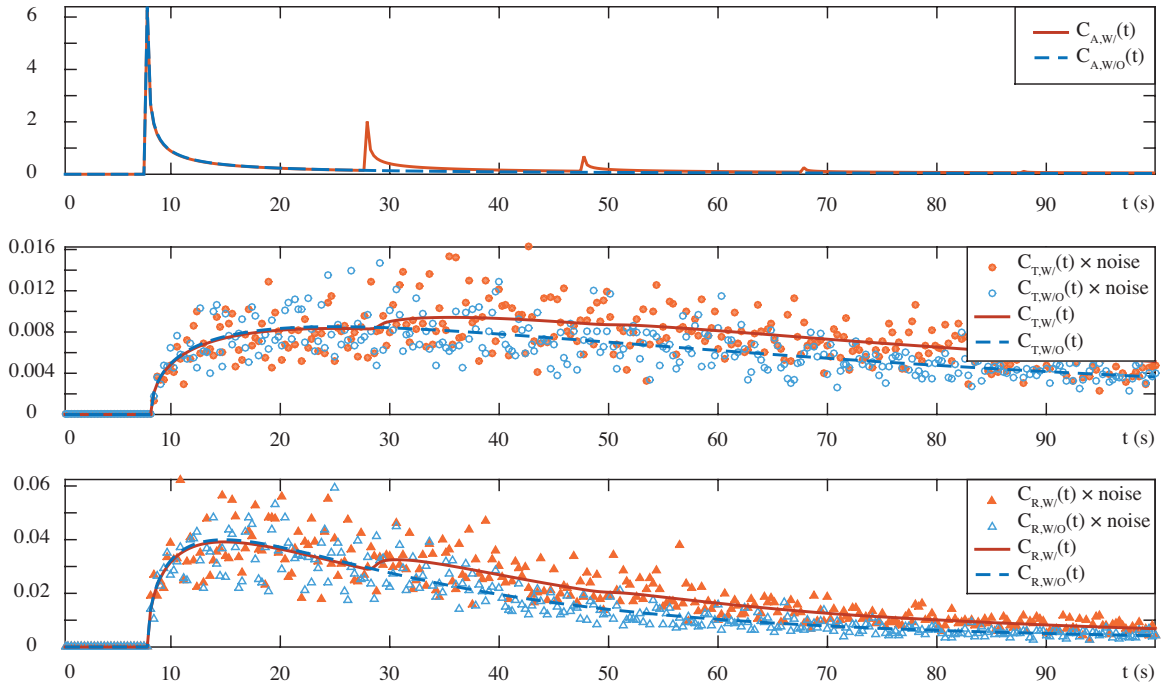

Figure 5-1: Simulated TICs with (orange) and without recirculation (blue) corresponding to noise-free AIF (top), examples of noise-free and noisy TICs in the fourth tissue region (middle) and in the reference tissue (bottom). The first hundred seconds are displayed here.

and N_R is the number of recirculation loops which are taken into account. The TIC, $C_{A1}(t)$, thus represents the AIF without recirculation.

To go further in the simulation process, a simplified recirculation model was defined, assuming a constant recirculation period γ, a constant recirculation fraction β (the fraction of microbubbles remaining from the previous bolus pass taking into account bubble disruption and filtration), a constant spread factor α through the different recirculation loops, and an exponential spread and decay of the signal. The r$^{\text{th}}$ recirculation TIC, $R_r(t)$, was simulated by equation 5.3:

$$R_r\left(t - r\gamma\right) = \frac{\beta^r}{\alpha^r} C_{A1}\left(\frac{t}{\alpha^r}\right) \tag{5.3}$$

Examples of AIF with and without recirculation are shown in Figure 5-1 (first row). For the present study, $C_{A1}(t)$ is represented by a log-normal function, $C_{Aw}(t)$ is computed using $\alpha = 2$, $\beta = 30\%$, $\gamma = 20$ s and $N_R = 7$. TICs were simulated for a total duration of 165 s with a frame rate of 3 Hz.

5.3.3 Noise model

A multiplicative noise model following a gamma distribution [1] while constraining the mean intensity to be 1 (unit mean). Indeed, a unit mean distribution for a multiplicative noise is the equivalent of a zero-centered distribution for additive noise. A gamma distribution is defined by two parameters: its shape parameter κ, and its scale parameter θ. Enforcing a unit mean is equivalent to set $\theta = 1/\kappa$, the noise distribution $p(v)$ is then defined by Eq. 5.4:

$$p(v) = 1/\Gamma(\kappa)\ \kappa^{\kappa}\ v^{\kappa-1}\ e^{-v\kappa},\ \forall\ v \geq 0. \tag{5.4}$$

The parameter κ controls the sharpness of the noise distribution, and is related to the standard deviation of the noise ditribution by $\sigma = 1/\sqrt{\kappa}$.

5.3.4 Perfusion quantification methods

Six perfusion quantification methods ($M_1 - M_6$) were tested and compared. Among them, four relative approaches ($M_3 - M_6$) making use of an in-plane reference tissue (R) were proposed to make parameters more robust to inter-exam changes (due to unavoidable experimental or physiological varying conditions). Furthermore, the last method (M_6) takes advantage of the multiple regions that can be defined inside an image.

Methods M_1 and M_2 - Log-Normal model (LN)

The Log-normal function is an explicit model that depends on four parameters, it is frequently used to fit TICs, in particular from dynamic contrast-enhanced ultrasound studies [11]. From this model, the area under the curve AUC_i, which is proportional to the tissue blood volume (see Appendix for proof) and τ_i a time parameter reflecting the delay between the beginning of the acquisition and the arrival of the first microbubbles in the tissue of interest are directly estimated. In addition, the wash-in rate (WIR_i), that is the maximal slope of the uptake part of the TIC, a parameter related to the tissue blood flow (see Appendix for proof), is commonly derived. Appendix shows the analytical expression of the AUC and WIR parameters, using the conventional expression of the Log-Normal model. For the first

method (M_1), all the time samples are analyzed while for the second model (M_2), the analysis is restricted to the first pass of the bolus, which roughly corresponds to the wash-in phase.

Methods M_3 and M_4 - relative Log-Normal model (rLN)

The relative Log-Normal models propose the comparison of the LN model parameters estimated in the tissue region i (AUC_i, WIR_i, and τ_i) with the corresponding values estimated in the reference tissue R (AUC_R, WIR_R, and τ_R), following equation 5.5:

$$rAUC_i = \frac{AUC_i}{AUC_R}, rWIR_i = \frac{WIR_i}{WIR_R}, \Delta = \tau_i - \tau_R. \tag{5.5}$$

For the method M_3, all the time samples are analyzed while for the method M_4, the analysis is restricted to the first pass of the bolus.

Methods M_5 - relative one-compartment model (rLin)

The model M5 is derived from the one-compartment model presented in Section 5.3.1. It was proposed to take into account the multiple cases for which the estimation of the AIF is tricky, see for instance [6]. It assumes that the tissue region and the reference tissue are parallel single compartments, fed by a common AIF. Writing equation (5.1) respectively for C_{T_i} and C_R, and rearranging them, a convolution equation that is independent of the AIF can be deduced. Four related perfusion parameters [6], defined by Eq. 5.6, can then be estimated as a linear function:

$$rF_i = F_i/F_R, rV_i = V_i/V_R, k_i = F_i/V_i, \delta_i = D_i - D_R. \tag{5.6}$$

When the time delay δ_i is estimated (defined as the inflexion point after temporal filtering), the convolution equation can be written as follows:

$$W_i(t) = rF_i \cdot X(t) + rV_i \cdot k_i \cdot Y(t) - k_i \cdot Z_i(t), \forall t \geq \delta_i. \tag{5.7}$$

with $W_i(t) = C_{T_i}(t-\delta_i)$, $X(t) = C_R(t-\delta_R)$, $Y(t) = \int_0^t C_R(\tau - \delta_R)\,\mathrm{d}\tau$, and $Z_i(t) = \int_0^t C_{T_i}(\tau - \delta_i)\,\mathrm{d}\tau$. The three parameters rF_i, rV_i, and k_i can thus be estimated using a linear regression which

minimizes the least-squares error. For that reason the method M_5 is noted rLin. It was introduced in [5] following Patlak's approach [10].

Method M_6 - Regularized relative one compartment model (rReg)

This approach was proposed in [5] to overcome the limitations of the rLin model when it is applied to N (N being more than one) tissue regions. Indeed, the estimation of N values of rF_i, rV_i, and k_i provides N potentially different values of $k_R = F_R/V_R$, since $k_R = \frac{F_R}{F_T^i}\frac{F_T^i}{V_T^i}\frac{V_T^i}{V_R} = \frac{rV_i.k_i}{rF_i}$. The discrepancy of the values of k_R can be overcome by forcing this parameter to have the same value across the different regions, i.e. forcing a common ratio between $rV^i.k_T^i$ and rF^i across all tissue regions. In summary, an iterative estimation method was proposed, each iteration being conducted in two steps : first a value for k_R=$\frac{rV_i.k_i}{rF_i}$ is chosen, then the $3N$ values rF_i, rV_i, and k_i are estimated by applying N linear optimization processes under constraints, this two-step procedure being repeated in order to minimize a global error term defined as the sum of the N errors of the N fittings. As compartmental approaches take into account recirculation inherently, the truncature approach defined for Log-Normal based models was not tested for models M_5 and M_6.

5.4 Experimental design

5.4.1 Simulations

Simulations were derived from the small animal experiments described in [6]. For that study, the tumor area was divided into 32 regions (N = 32) and a reference tissue were considered, yielding 33 TICs. For the present study, two sets of 33 TICs were generated, using two different arterial input functions: $C_{A1}(t)$, based on a log-normal model, and $C_{Aw}(t)$, directly derived from $C_{A1}(t)$ according to equation (5.2) to simulate recirculation (Figure 5-1). Reference perfusion parameters F_i, V_i, D_i, V_R, F_R, and D_R, displayed on Figure 5-2, were chosen according to values estimated on an experimental dataset. The (N + 1) TICs C_{T_i} and $C_R(t)$ were simply derived using equations (5.1) and (5.4). Fig. 5-1 shows two examples of such simulated TICs. For each configuration (without and with recirculation), noise-free and noisy

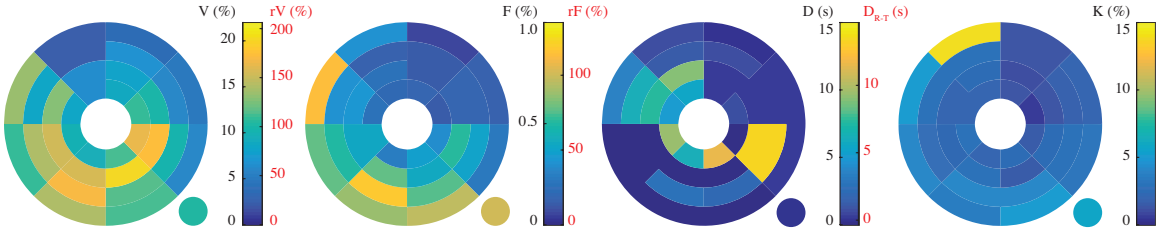

Figure 5-2: Bull's-eyes representation of the perfusion parameters used to simulate the 32 regional TICs, C_{T_i} (large circle), and the reference TIC, C_R (bottom right disk). From left to right: tissue blood volume (V), tissue blood flow (F), time-delay (D), and rate constant (k). The scale displayed in red color shows relative parameters: rV, rF, δ as defined by Eq. (5.6).

TICs were simulated (see Figure 5-1. Ten noise levels with σ varying from 0.05 to 0.5 were defined and in each case, 150 realizations were considered. A Log-Normal model was fitted to each simulated noise-free C_{T_i} TIC (generated using $C_{A1}(t)$), yielding reference values for AUC_i, WIR_i and τ_i.

5.4.2 Data analysis

For each simulated TIC $C_{hi}^{nj}(t)$, associated with configuration h (for $h = 1$, the AIF is $C_{A1}(t)$, for $h = 2$ the AIF is $C_{Aw}(t)$), region i ($i = 1, \ldots, 32$), noise level n ($n = 0, \ldots, 10$) and realization j ($j = 1, \ldots, 150$), the different perfusion parameters $\Theta_{hi}^{nj}(M_m)$ were estimated using the six methods (M_m, $m = 1, \ldots, 6$) presented in Section 5.3.4. As the methods M_2 and M_4 were defined to be less sensitive to recirculation, the LN model was fitted to the 20 first seconds following the time-delay estimated for each TIC, since $\gamma = 20$ seconds was the recirculation period used for simulation.

For parameters related to the tissue blood flow or to the tissue blood volume, the relative estimation error, expressed in %, was defined as follows:

$$E_{hi}^{nj}(M_m) = \frac{\Theta_{hi}^{nj}(M_m) - \Lambda_i(M_m)}{\Lambda_i(M_m)} \tag{5.8}$$

where $\Lambda_i(M_m)$ is the reference value of the perfusion parameter estimated in the i^{th} tissue region using method M_m. For time-delay parameters the absolute estimation error was

defined in seconds as:

$$E_{hi}^{nj}(M_m) = \Theta_{hi}^{nj}(M_m) - \Lambda_i(M_m), \tag{5.9}$$

5.5 Results

Fig. 5-3 shows statistical results related to the perfusion parameters estimated inside one specific region ($i = 4$) using the six models (M_m) described in section 5.3.4, $\Theta_{h4}^{n}(M_m)$. Indeed, the simulated values $\Lambda_4(M_m)$ and the median, first, and third quartile values over the 150 simulations of parameters are represented as a function of the noise level (indice n, proxied by σ). These results are displayed for simulations without ($h = 1$) and with recirculation ($h = 2$).

In complement to Fig. 5-3, Fig. 5-4, 5-5, and 5-6 display bull's-eye representations of the median estimation errors in the 32 regions for an intermediate noise level ($\sigma = 0.25$, $n = 6$), $E_{hi}^{6}(M_m)$, for the six quantification methods and the two conditions of recirculation.

5.5.1 Model M_1

When focusing on data without recirculation, the LN model (model M_1) is robust, it estimates accurate values of AUC_i and WIR_i, whatever the level of noise. In particular, the intermediate noise level yields relevant estimates in all tissue regions. The time delay seems to be the less robust parameter but does not impact the reliability of the other parameters. When introducing the recirculation model, the estimation of AUC_i ($E \geq 25\%$), and in a less extent the estimation of WIR_i ($E \leq 15\%$) are biased, but the bias does not vary with noise. As for the estimation of time-delays, behaviors similar to the LN model without recirculation can be observed.

5.5.2 Model M_2

When using the LN model restricted to the wash-in phase (model M_2), both AUC_i and WIR_i parameters are respectively largely under and over estimated, whatever the configuration, i.e. without and with recirculation. Some disparities exist between regional parameters: the

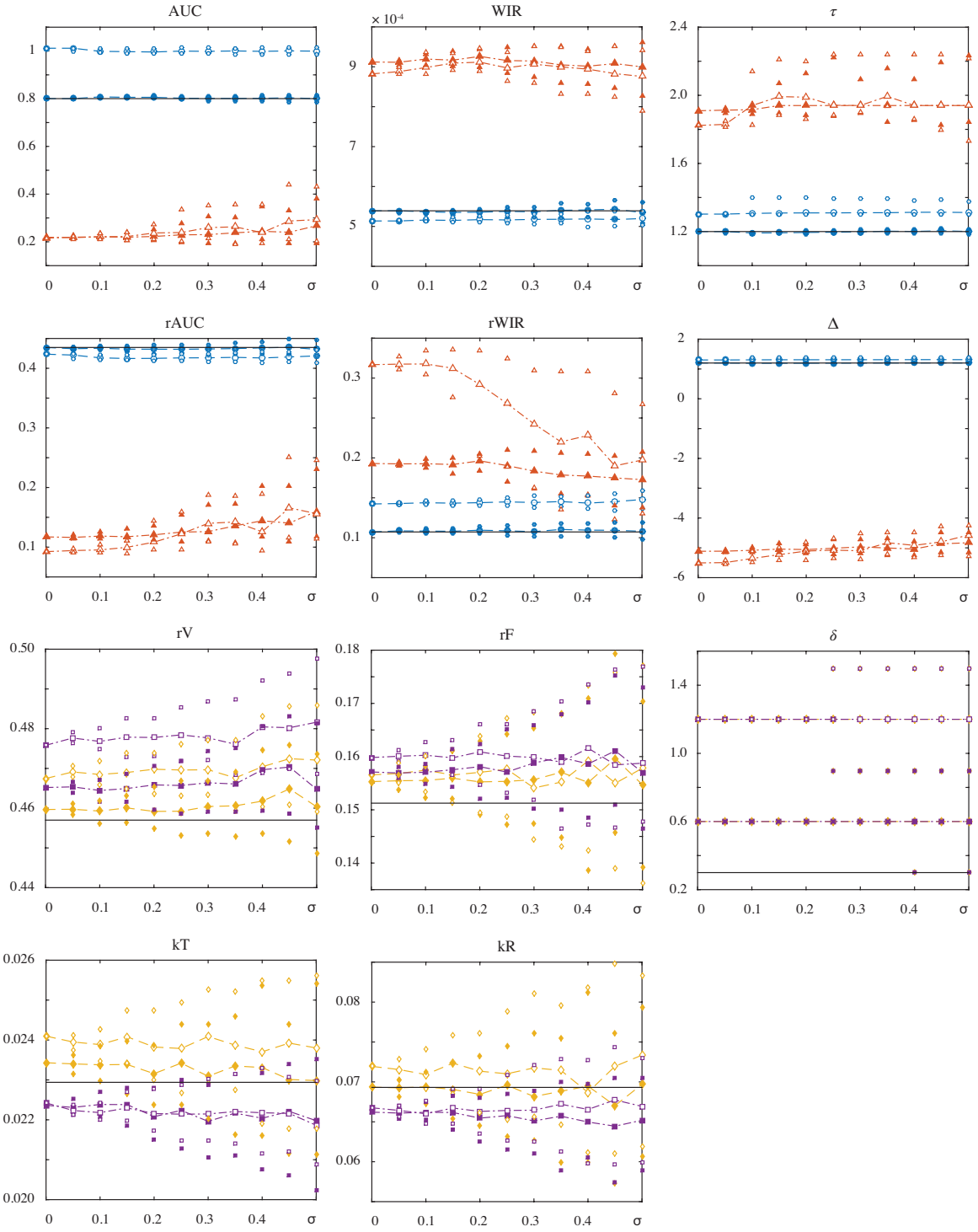

Figure 5-3: Median values (large symbols), first and third quartiles (small symbols) of parameters estimated for the fourth tissue region C_{T_4} (outer ring, upper halve, right octant). First column: tissue blood volume related parameters, second column: tissue blood flow related parameters, third column: time-delay related parameters, fourth row: rate constants in the tissue region and reference tissue. Constant lines in black represent simulated values, blue lines the estimation corresponding to the LN model, red lines the estimation corresponding to the LN model restricted to wash-in phase. Yellow color stands for rLin model, while purple color stands for rReg model. For all of the cases, filled symbols correspond to the configuration without recirculation, while empty symbols correspond to the configura-

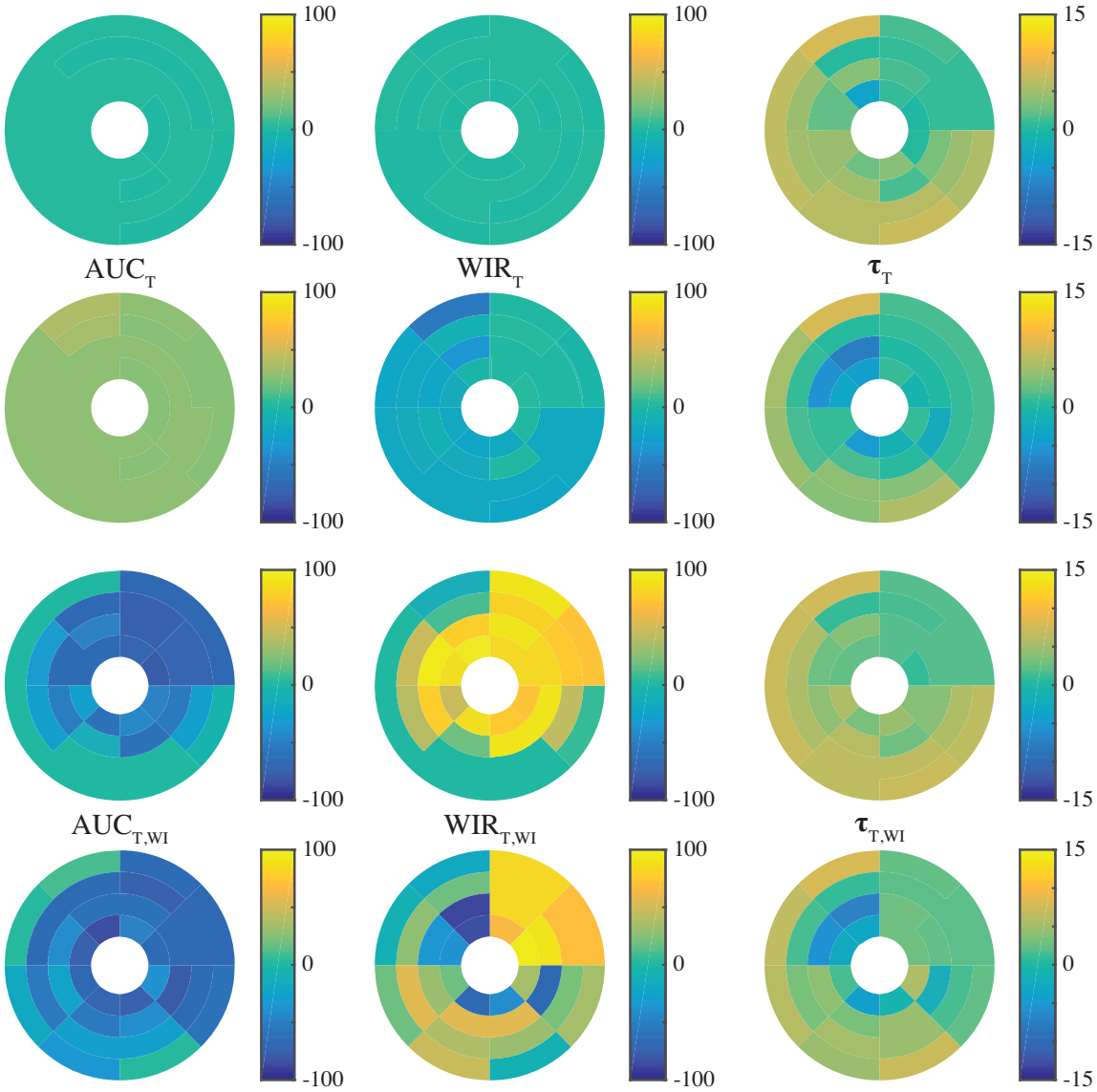

Figure 5-4: Bull's-eyes of the median estimation errors obtained by the LN model at the intermediate noise level. From left to right: estimation errors corresponding to tissue blood volume, tissue blood flow, time delay. From top to bottom: M_1 without recirculation, M_1 with recirculation, M_2 without recirculation, M_2 with recirculation.

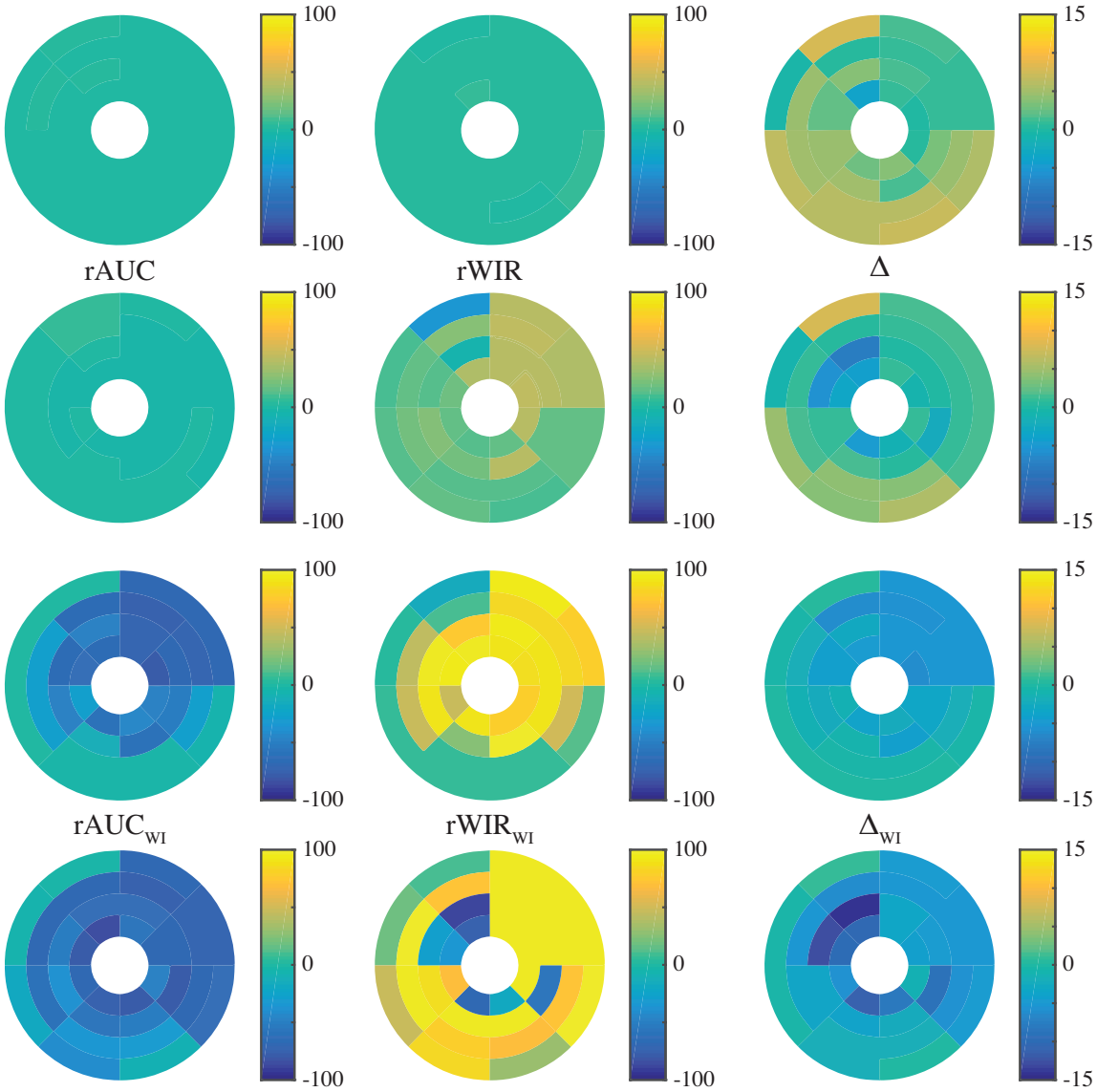

Figure 5-5: Bull's-eyes of the median estimation errors obtained by the rLN model at the intermediate noise level. From left to right: errors corresponding to tissue blood volume, tissue blood flow, time delay. From top to bottom: M_3 without recirculation, M_3 with recirculation, M_4 without recirculation, M_4 with recirculation.

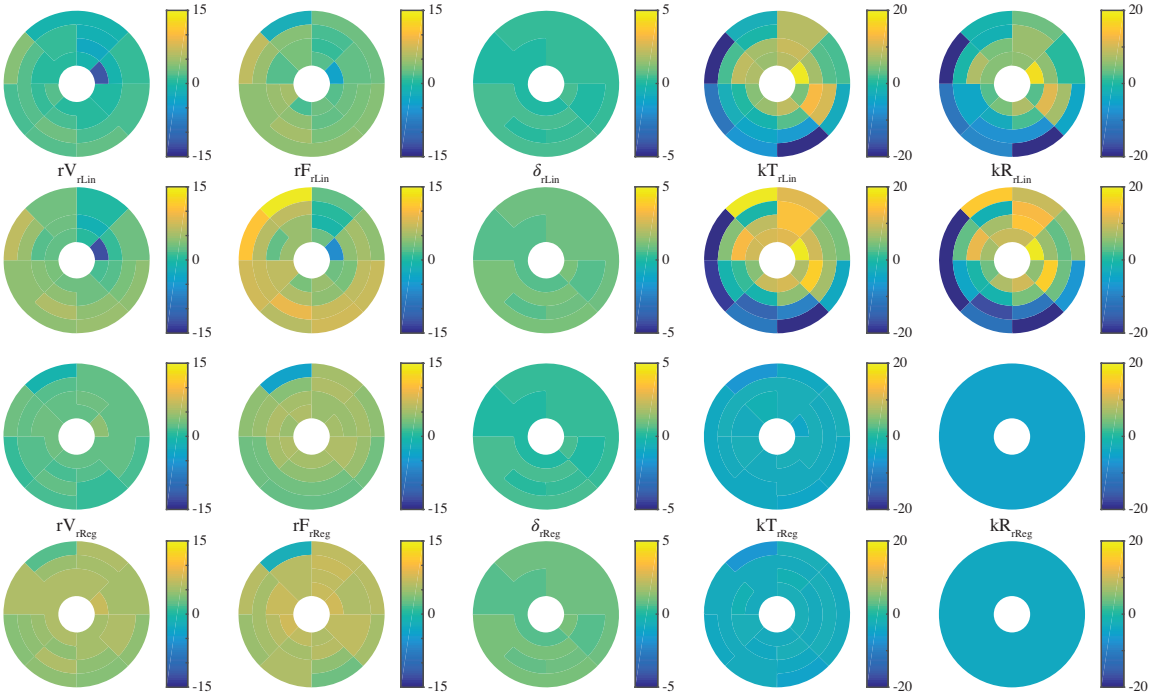

Figure 5-6: Bull's-eyes of the median estimation errors obtained by the rLin and rReg models at the intermediate noise level. From left to right: errors corresponding to tissue blood volume, tissue blood flow, time delay, rate constant in tissue regions, rate constant in the reference tissue deduced from the different estimations inside tissue regions. From top to bottom: M_5 without recirculation, M_5 with recirculation, M_6 without recirculation, M_6 with recirculation.

smallest values of tissue blood flow or tissue blood volume tend to provide larger relative estimation errors.

5.5.3 Model M_3

As expected, the rLN model (model M_3) for data without recirculation is robust, and provides accurate values of $rAUC_i$ and $rWIR_i$, whatever the level of noise and for the intermediate noise level, and the estimation is relevant in all regions. As could be anticipated, introducing recirculation, the estimation of $rAUC_i$ was rather accurate but the estimation of $rWIR_i$ was biased (bias invariant with noise), especially for smaller values of simulated tissue blood flow.

5.5.4 Model M_4

When using the rLN model restricted to the wash-in phase (model M_4), both $rAUC_i$ and $rWIR_i$ parameters were respectively largely under and over estimated, whatever the configuration: without and with recirculation. Results show similar trends to those observed when using the LN model restricted to the wash-in phase (model M_2).

5.5.5 Model M_5

The rLin model (model M_5) accurately estimates relative tissue blood volume and relative tissue blood flow parameters, exhibiting small biases, but the precision depends on the noise level. The estimation of time delays parameters appears to be robust. Biases are larger when taking into account studies with recirculation, but remain in most cases moderate ($E \leq 15\%$). Considering rate constants, some heterogeneity in estimated k_R values was found. This confirms our assumption, since no constraints are applied to this specific values. Moreover, related errors appear in the estimates of k_{T_i}.

5.5.6 Model M_6

Compared with the model M_5, results using model M_6 are improved. By construction, a constant value of k_R is estimated for all the subregions (slightly underestimated in the case shown in Figure 5-6), and consequently the relative error in the estimation of k_{T_i} is highly homogeneous across tissue regions and almost constant. Indeed the largest median relative error on k_{T_i} is observed for the highest value of simulated k_{T_i}. The rReg model estimates relative blood flow parameters and relative blood tissue parameters, with median relative errors generally less than 5% without recirculation for the intermediate noise level (see Fig. 5-6). Of course, recirculation yields higher estimation errors, nevertheless they remain below 7% in most cases and appear to be more homogeneous across the 32 subregions than the estimates of model M_5.

5.6 Discussion

This study aimed at comparing the behavior of different models suitable for quantification of perfusion in contrast-enhanced ultrasound studies. Our whole analysis was based on simulated studies in order to have an irrefutable gold standard and to compare the different methods in terms of precision and accuracy. The model describing contrast displacement relies on a one-compartment model, that has proved to be valid to describe contrast enhancement in a murine tumor model [6]. In order to introduce some variations in the tissue blood flows, tissue blood volumes and time-delays, reflecting the regional heterogeneity among tissue regions, as observable with ultrasound. N regions inside the simulated tissue of interest were introduced, each one being characterized by its set of perfusion parameters. In addition an arterial input function was first simulated using a single Log-Normal function, then approximated by a sum of modified Log-Normal functions to mimic recirculation. Although the deformation of the first-pass is quite simplistic, this approach enables us to consider two configurations: one idealized configuration without recirculation and one configuration closer to physiological conditions introducing recirculation. Finally different signal to noise conditions were simulated using a multiplicative noise model, as opposed to an additive Gaussian model, reflecting conditions encountered in contrast-enhanced ul-

trasound. Using 150 noisy simulations for each condition guarantees a representative set of possibilities, allowing generalization of the results, as well as enabling the study of the precision of the estimations.

The use of median and quartile operators to assess the estimation errors was necessary to reduce the impact of outliers, which were mostly found in the estimates of the rLin model. Using relative estimation errors (as opposed to absolute estimation errors) for tissue blood flows and tissue blood volumes related parameters allows easy comparison of the errors obtained for parameters with different simulated values.

As expected, results of this study exhibit lower precision of the estimated parameters with decreasing signal to noise ratio. Interestingly, most of the methods are not strongly affected by the signal to noise ratio in terms of accuracy (reflected by the median error on parameters). In addition, perfusion parameters were found less accurate when estimated with recirculation, compared to the estimates without recirculation.

The Log-Normal model, when applied to the whole duration of the study is robust to noise. However this model is subject to recirculation error. To get rid of this dependency, a naive approach consists in limiting the estimation of Log-Normal model to the first samples of the TIC (before recirculation occurs). However this solution appears to be unstable, providing estimates with huge discrepancies when compared to simulated parameters and also showing a large dependency to noise. This naive approach should therefore be absolutely avoided when dealing with dynamic perfusion data. Indeed results are not accurate for both configurations, i.e. with or without recirculation. Thus the present simulation study also emphasizes the need for acquisitions with sufficiently long durations in order a reliably estimate perfusion parameters, and in particular when relying on the Log-Normal model for quantification.

The use of a reference tissue to normalize perfusion parameters was already recommended following a test-retest study that was conducted on dynamic contrast-enhanced ultrasound acquisitions performed on small animals [6]. Normalization was also proposed by a clinical study in order to enable the comparison of perfusion parameters estimated using contrast-enhanced ultrasound data and contrast-enhanced computerized tomography [8]. The present simulation study confirms the interest of normalization when looking at the

accuracy and the precision of estimated parameters. Despite the use of the division operator that could be impacted by noise issues, normalized parameters are more accurate than "absolute" parameters when introducing recirculation in simulated TICs. As recirculation is physiological and cannot be suppressed experimentally, our results emphasis the need to address this question when dealing with real data.

Comparing the estimation of relative parameters using the rLN model, it appears that the $rAUC$ parameter is more precise than the $rWIR$ parameter. This experimental result is in concordance with the theory, as detailed in the appendix section of this paper. The differences which are observed between the estimated and simulated values of $rAUC$ in case of recirculation can partly be explained by the fitting of a Log-Normal model to the reference tissue prior to quantification. This step is useful to reduce the impact of noise but slightly inaccurate to represent TICs with recirculation, the use of a model-free noise-filtering technique should be investigated. To summarize it is important to note that in case of recirculation, the $rAUC$ is more representative of the simulated parameters than AUC.

The linear resolution of the relative one-compartment approach (method M_5) was introduced to process contrast-enhanced ultrasound studies in [5]. It ensures the fitting error reaches its global minimum, as opposed to the non-linear approach used in [6]. Furthermore, linear resolution significantly reduces computing-time. Some aberrant values of perfusion parameters can however be found since parameters were not bounded during the estimation process. As indicated in the theory section, applying this method independently to multiple regions yields multiple values of k_R, this effect was also shown in Figure 5-3 and Figure 5-6. Method M_6 simply enforces a single value of k_R should be estimated across tissue regions. As a consequence, the approach yields spatially regularized estimates of k_T, slightly biased. As expected, the impact of recirculation on estimates of models M_5 and M_6 is rather low, however not negligible. This effect could be partly explained by the approximation of the TIC inside the reference tissue by the Log-Normal model which does not account for recirculation. This prior modeling was performed in order to reduce the impact of noise on the relative perfusion parameters. The median relative errors on these parameters are all less than 7%, even in presence of recirculation, which acceptable. This is illustrated in Figure 5-6 for an intermediate noise level.

The estimation of absolute values of perfusion parameters is possible, at least theoretically. It would however require an accurate estimation of the arterial input function. Its proper estimation from image data is a large research question which is not fully solved, even considering other perfusion imaging modalities such as MRI or PET. Some problems are inherent to ultrasound data, ranging from the calibration of signal intensity according to the amount of injected contrast agent, to issues resulting from the 2D nature of data. Additionally, the estimation of such a function in small vessels, surrounding a tumor for instance, is subject to partial volume effects, along with small displacements effects. Therefore, when quantifying CEUS data, we recommend using relative parameters, i.e. parameters normalized according to a reference tissue. Indeed, the chosen reference tissue should be accessible and rather homogeneous. However the robustness of the rLin and rReg models to the choice of the reference tissue remains to be fully investigated.

5.7 Conclusion

This study was designed to investigate the impact of recirculation on the quantification of contrast-enhanced ultrasound exams, by means of simulations based on experimental data. Fitting a Log-Normal model on the first pass of the bolus implies a reduction of the number of points used to fit the model and yields unstable estimates, especially on noisy data. This solution is thus inappropriate. Modeling methods such as compartmental modeling, that account for recirculation intrinsically, are indeed the most robust to recirculation. Making use of a reference tissue, the estimation of relative parameters appears to be robust. Taking advantage of the multiple regions, and enforcing estimation of a single rate constant characterizing the reference tissue, provides stable estimates, especially when comparing parameter estimates across regions. This approach is therefore recommended because of its reduced sensitivity to recirculation, and better homogeneity of the estimates inside the considered field of view.

Appendix

Taking into account the generic expression of the Log-Normal model:

$$\frac{A}{\sqrt{2\pi}\sigma(t-\tau)}\exp\left(-\frac{\left[\ln\left(t-\tau\right)-\mu\right]^2}{2\sigma^2}\right)$$

and considering the formal definitions of the area under the curve and of the wash-in rate, it can be deduced:

$$\begin{aligned} AUC &= A \\ WIR &= \frac{A}{\sigma\sqrt{2\pi}}\left(\frac{y}{\sigma^2}-1\right)e^{2y-2\mu-\frac{y^2}{2\sigma^2}} \\ \text{with} \quad y &= \frac{3\sigma^2+\sigma\sqrt{\sigma^2+4}}{2} \end{aligned}$$

These equations were directly used to compute the AUC and WIR parameters from a Log-Normal approximation.

AUC and WIR can also be derived when considering a one-compartment vascular model, their expression is computed for two cases in the following table: one simplified case assuming that $C_A(t)$ follows a gate function and the general case. In addition relative parameters $rAUC$ and $rWIR$ are formally computed when considering a reference tissue. Using the gate function for $C_A(t)$ shows a strong equivalence between AUC and tissue blood volume V, but also between WIR and tissue blood flow F. Thus, for that case, $rAUC = rV$ and $rWIR = rF$. Using the general shape for $C_A(t)$ shows that AUC is strictly proportional to V, and that $rAUC = rV$. Furthermore, WIR is related to F, but $rWIR$ is not strictly identical to rF, since a corrective factor ρ is introduced. This factor depends of the time of inflexion (denoted t_I) of each TIC and explains why the $rWIR$ is generally not strictly equivalent to rF.

AIF	$Krect_a(t)$	$C_A(t)$
AUC	KV_T	$V_T \int_0^{+\infty} C_A(\tau)\,\mathrm{d}\tau$
WIR	$\frac{KF_T}{a}$	$F_T\left(C_A(t_I) - \frac{1}{V_T} C_T(t_I - D_T)\right)$ $\left\{t_I \mid \frac{\mathrm{d}C_T}{\mathrm{d}t}(t_I - D_T) = V_T \frac{\mathrm{d}C_A}{\mathrm{d}t}(t_I), \frac{\mathrm{d}C_A}{\mathrm{d}t}(t_I) > 0\right\}$
$rAUC$	rV	rV
$rWIR$	rF	$\rho \cdot rF$

Table 5.1: Analytic expressions of perfusion parameters using a one-compartment model and assuming two different shapes of AIF: rectangle function of width a and height $1/a$, $rect_a(t)$, and general case $C_A(t)$. In the first case, K stands for the injected concentration.

Bibliography

[1] Guillaume Barrois, Alain Coron, Thomas Payen, Alexandre Dizeux, and S Lori Bridal. A Multiplicative Model for Improving Microvascular Flow Estimation in Dynamic Theory and Experimental Validation. *IEEE Trans. Ultrason., Ferroelect., Freq. Contr.*, 60(11): 2284–2294, 2013. 86

[2] M J Blomley and P Dawson. Bolus dynamics: theoretical and experimental aspects. *Br J Radiol*, 70(832):351–359, April 1997. 84

[3] Julio Cárdenas-Rodríguez, Christine M Howison, and Mark D Pagel. A linear algorithm of the reference region model for DCE-MRI is robust and relaxes requirements for temporal resolution. *Magn Reson Imaging*, 31(4):497–507, May 2013. 83

[4] C F Dietrich, Michalakis Averkiou, J-M Correas, N Lassau, E Leen, and F Piscaglia. An EFSUMB introduction into Dynamic Contrast-Enhanced Ultrasound (DCE-US) for quantification of tumour perfusion. *Ultraschall Med*, 33(4):344–351, August 2012. 82

[5] Maxime Doury, Alexandre Dizeux, Alain De Cesare, Olivier Lucidarme, S Lori Bridal, and Frédérique Frouin. Regularized linear resolution of a one-compartment model to improve the reproducibility of perfusion parameters in CEUS. In *2016 IEEE International Ultrasonics Symposium (IUS)*, pages 1–4. IEEE, 2016. 83, 88, 98

[6] Maxime Doury, Alexandre Dizeux, Alain De Cesare, Olivier Lucidarme, Claire Pellot-Barakat, S Lori Bridal, and Frédérique Frouin. Quantification of tumor perfusion using dynamic contrast-enhanced ultrasound: impact of mathematical modeling. *Phys Med Biol*, 62(3):1113–1125, February 2017. 83, 84, 87, 88, 96, 97, 98

[7] R N Gunn, S R Gunn, and V J Cunningham. Positron emission tomography compartmental models. *J Cereb Blood Flow Metab*, 21(6):635–652, June 2001. 84

[8] Thibaud Lefort, Frank Pilleul, Sébastien Mulé, S Lori Bridal, Frédérique Frouin, Catherine Lombard-Bohas, Thomas Walter, Olivier Lucidarme, and Aymeric Guibal. Correlation and agreement between contrast-enhanced ultrasonography and perfusion computed tomography for assessment of liver metastases from endocrine tumors: normalization enhances correlation. *Ultrasound Med Biol*, 38(6):953–961, 2012. 97

[9] MR Lowerison, JJ Tse, MN Hague, AF Chambers, DW Holdsworth, and JC Lacefield. Compound speckle model detects anti-angiogenic tumor response in preclinical nonlinear contrast-enhanced ultrasonography. *Med Phys*, 44(1):99–111, 2017. 83

[10] Clifford S Patlak, Ronald G Blasberg, and Joseph D Fenstermacher. Graphical evaluation of blood-to-brain transfer constants from multiple-time uptake data. *J Cereb Blood Flow Metab*, 3(1):1–7, March 1983. 88

[11] Costas Strouthos, Marios Lampaskis, Vassilis Sboros, Alan McNeilly, and Michalakis Averkiou. Indicator dilution models for the quantification of microvascular blood flow with bolus administration of ultrasound contrast agents. *IEEE Trans Ultrason Ferroelectr Freq Control*, 57(6):1296–1310, June 2010. 82, 86

[12] Simona Turco, Hessel Wijkstra, and Massimo Mischi. Mathematical Models of Contrast Transport Kinetics for Cancer Diagnostic Imaging: A Review. *IEEE Reviews in Biomedical Engineering*, 9:121–147, 2016. 82

[13] Thomas E Yankeelov, Jeffrey J Luci, Martin Lepage, Rui Li, Laura Debusk, P Charles Lin, Ronald R Price, and John C Gore. Quantitative pharmacokinetic analysis of DCE-

MRI data without an arterial input function: a reference region model. *Magn Reson Imaging*, 23(4):519–529, May 2005. 83

Appendix A

Abbreviations and reference data